LE JOURNAL DE PHYSIQUE

TOME 40, SEPTEMBRE 1979, PAGE 819

Classification
Physics Abstracts
33.10 — 33.20F — 33.35 — 33.70 — 33.80K — 42.65C

Line shape and Doppler broadening in resonant CARS and related nonlinear processes through a diagrammatic approach

S. A. J. Druet, J.-P. E. Taran

ONERA, 92320 Châtillon, France

and Ch. J. Bordé

Laboratoire de Physique des Lasers, Université Paris-Nord, 93430 Villetaneuse, France

(*Reçu le 28 mars 1979, accepté le 15 mai 1979*)

Résumé. — Nous étudions l'influence de la résonance électronique sur les largeurs de raies de la Diffusion Raman Anti-Stokes Cohérente (DRASC) dans les gaz à faible pression. D'autres processus non linéaires du 3^e ordre sont aussi examinés. Nous avons effectué une étude théorique de tous ces phénomènes en utilisant une représentation diagrammatique des polarisations non linéaires. Les diagrammes permettent de classer aisément les différents processus physiques qui contribuent à la création de la polarisation non linéaire, et de calculer rapidement grâce à des règles simples les termes correspondants de la susceptibilité. En DRASC, les termes de la susceptibilité qui dominent en régime Doppler (parce qu'ils ne subissent pas d'élargissement Doppler) diffèrent de ceux qui dominent en régime collisionnel. Ceci entraîne d'importantes différences entre les contenus spectraux des régimes Doppler et collisionnel. Au contraire, en diffusion Stokes cohérente ainsi qu'en diffusion Raman stimulée, ce sont les mêmes termes qui dominent dans les deux régimes. Nous traçons quelques formes de raies types. Nous montrons qu'il est aisé de généraliser cette étude à tous les processus non linéaires.

Abstract. — We examine the effect of electronic resonance enhancement on the line broadening for Coherent Anti-Stokes Raman Scattering (CARS) and related third-order non linear processes, in low pressure gases. These phenomena are analysed theoretically within the framework of a time-ordered diagrammatic representation of nonlinear polarizations. Diagrams facilitate the classification of the various physical processes and provide a way to readily derive all the susceptibility contributions. In CARS, the susceptibility terms which are Doppler-free and thus prevail in the Doppler limit are different from those which dominate in the collision broadening regime. This causes important changes in the spectral content. On the contrary, the same terms are seen to dominate, in both regimes, in coherent Stokes Raman scattering or in stimulated Raman scattering. Typical line contours are displayed. The generalization to all nonlinear processes is outlined.

1. **Introduction.** — One of the finest achievements of Coherent Anti-Stokes Raman Scattering, or CARS [1, 2], is the high-resolution near Doppler- free Raman spectroscopy of gases [3-7]. The reduction in Doppler broadening for CARS results from the forward scattering character of the process : the Doppler shifts of the applied collinear pump waves at ω_1 and ω_2 are of the same order in the frame of a moving molecule. Consequently, if the difference $\omega_1 - \omega_2$ is tuned to the Raman transition ω_{ba} of a molecule at rest (Fig. 1), this difference is also approximately at resonance with ω_{ba} whatever the axial velocity of the molecule. Strictly speaking, a residual Doppler broadening remains with a width which is of the order of $\omega_{ba}(2\,k_B\,T/Mc^2)^{1/2}$, where T is the temperature, M the mass of the molecule and k_B the Boltzmann constant. This effect has been demonstrated experimentally and studied theoretically [3, 4, 7-10]. The problem that we address here is the influence of possible resonances between any of the three light frequencies involved in CARS (ω_1, ω_2 and $\omega_3 = 2\,\omega_1 - \omega_2$) and any of the allowed one-photon optical transitions of the molecules : such additional resonances may affect the line contours in the Doppler broadening regime.

A recent investigation of molecular resonant CARS

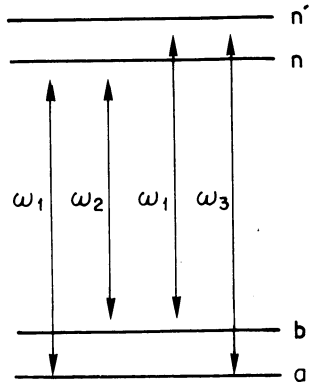

Fig. 1. — Energy level diagram for CARS ; a, b are the rovibrational states pertaining to the ground electronic state and coupled by the Raman transition ω_{ba} ; n, n' are rovibrational states pertaining to the excited electronic state ; ω_1 and ω_2 are the pump frequencies and $\omega_3 = 2\,\omega_1 - \omega_2$ is the anti-Stokes frequency.

spectroscopy has established that the spectra contain, for the most part, three distinct families of lines [2, 11, 12], with intensities which depend upon the population of the lower Raman level a. We shall examine in section 3 the line contours for these three families, and also the contours of the hot lines associated with the upper Raman level b. The theory is discussed in the case of mixed broadening (collisional + Doppler). The discussion is done in the framework of the time-ordered diagrammatic representation of nonlinear polarizations, which has been used recently for resonant CARS in the pure collision broadening limit [2, 12, 13] as well as for saturation spectroscopy and Doppler-free two-photon spectroscopy [14-17]. We show that not all CARS lines are Doppler-free, which is in contradiction to what was speculated in ref. [11]. Doppler broadening in off-resonance CARS is also discussed briefly : we confirm the recent results of Henessian and Byer [9].

We also show that a representation of the time-ordered processes in energy-momentum space allows us to readily determine if any given nonlinear process is subject to Doppler broadening [17, 18]. In this context, we establish the difference between true Doppler-free processes (such as two-photon absorption with counter-propagating beams), where all molecular velocity groups contribute equally, and particular processes (such as one-photon enhanced CARS and saturation spectroscopy) where a specific velocity group may give an overwhelming contribution of narrow width. Finally, the generalization to other classes of nonlinear optical processes of third order such as Stimulated Raman Scattering (SRS) and Coherent Stokes Raman Scattering (CSRS) is outlined.

2. **Mathematical Framework.** — 2.1 NONLINEAR POLARIZATION. — As is customary in CARS, we assume that the optical excitation is provided by two monochromatic plane waves, having the same polarization vector $\hat{e}$ aligned along the X axis, and propagating in the direction of the Z axis. The total applied electric field is written ([1]) :

$$\mathcal{E}(z, t) = \hat{e} \sum_{j=1,2} \tfrac{1}{2} E_j \exp i(-\omega_j t + k_j z + \varphi_j) + \text{c.c.} \quad (1)$$

In an isotropic medium such as the gas that we consider, the induced CARS polarization has the same polarization vector $\hat{e}$ and can be written :

$$\mathcal{P}^{(3)}(z, t) = \hat{e} \frac{P^{(3)}}{2} + \text{c.c.} \quad (2)$$

with ([2])

$$P^{(3)} = \tfrac{1}{4} \chi^{(3)}(-\omega_3, \omega_1, \omega_1, -\omega_2) \times \times E_1^2 E_2 \exp i(-\omega_3 t + k'_3 z + 2\varphi_1 - \varphi_2) \quad (3)$$

and $k'_3 = 2k_1 - k_2$; since the polarization vectors of $\mathcal{E}(z, t)$ and $\mathcal{P}^{(3)}(z, t)$ are parallel, the susceptibility $\chi^{(3)}(\omega_3)$ will be treated as a scalar from now on. Finally, we note that eqs. (1)-(3) are written in the laboratory frame.

On the other hand, the quantum state of the scattering molecules is represented by the density operator ρ, from which the CARS polarization will be obtained. Matters are, however, complicated by the molecular motions. Although these can be treated quantum mechanically for a rigorous treatment, it is sufficient here to take classical trajectories for the molecules, neglecting also relativistic effects. We can apply the treatment used by Bordé and coworkers for saturated absorption spectroscopy [14] ; we further assume that the velocities of the molecules are not changed during their interactions with the fields (i.e. we neglect the recoil effect) and we disregard velocity-changing collisions.

The density operator ρ is thus calculated for the class of molecules possessing velocity $\mathbf{v}$; an integration is then performed over the velocity distribution function $F(\mathbf{v})$:

$$\rho(\mathbf{r}, t) = \int \rho(\mathbf{r}, t, \mathbf{v})\, F(\mathbf{v})\, \mathrm{d}^3 v\,. \quad (4)$$

Here $\rho(\mathbf{r}, t, \mathbf{v})$ is the solution of the density operator evolution equation, which is, in the laboratory frame :

$$\frac{\partial}{\partial t} \rho(\mathbf{r}, t, \mathbf{v}) + \mathbf{v}.\nabla\rho(\mathbf{r}, t, \mathbf{v}) + R(\rho(\mathbf{r}, t, \mathbf{v}) - \rho^{(0)}) = = \frac{-i}{\hbar}[H_0 + V(t), \rho(\mathbf{r}, t, \mathbf{v})]\,, \quad (5)$$

([1]) The opposite convention for the time dependence of the complex representation of vectors is used by the authors of refs. [14-18].

([2]) We use electrostatic units throughout this paper. Our formulae are also valid in MKS, except eq. (3) where ε_0 must then be inserted as a multiplying factor to $\chi^{(3)}$ in the right-hand side.

for the class of molecules with velocity $\mathbf{v}$ ([3]); H_0 is the Hamiltonian for an unperturbed isolated molecule with a discrete spectrum of eigenstates $|\alpha\rangle$, $|\beta\rangle$, etc... corresponding to eigenenergies $\hbar\omega_\alpha$, $\hbar\omega_\beta$, etc. The Hamiltonian describing the interaction of the molecules with the radiation fields is

$$V(t) = -\boldsymbol{\mu}.\boldsymbol{\mathcal{E}}(z, t)$$

in the dipolar approximation and is treated as a perturbation. The term $R\rho$ gives a phenomenological representation of damping towards the equilibrium operator $\rho^{(0)}$, the operator R operating on ρ in the Liouville space. Finally, $\mathbf{v}.\nabla\rho(\mathbf{r}, t, \mathbf{v})$ is introduced into eq. (5) as a result of the Galilean transformation from the molecular frame to the laboratory frame. Because all k vectors are aligned along the Z axis, ρ depends only on the spatial coordinate z and on the velocity component v_z, so that we may write :

$$\mathbf{v}.\nabla\rho = v_z \frac{\partial\rho}{\partial z}. \tag{6}$$

The density operator components responsible for the CARS polarization are of order 3 with respect to the perturbation $V(t)$.

Molecules with axial velocity v_z thus give an elementary complex CARS polarization :

$$p^{(3)}(v_z) = 2N \operatorname{Tr}[\rho^{(3)}(\omega_3, z, t, v_z)\,\boldsymbol{\mu}.\hat{e}]$$
$$= 2N \sum_{\alpha,\beta} \rho^{(3)}_{\alpha\beta}(\omega_3, z, t, v_z)\,\mu_{\beta\alpha} \tag{7}$$

where $\rho^{(3)}(\omega_3, z, t, v_z)$ labels the Fourier component of $\rho^{(3)}(z, t, v_z)$ at frequency ω_3 : N is the number density, and the eigenstates $|\alpha\rangle$, $|\beta\rangle$, ... are assumed to be non-degenerate, so that the dipole operator $\boldsymbol{\mu}.\hat{e}$ has a single matrix element between each pair of states. The net polarization due to the ensemble of molecules is :

$$P^{(3)} = \int_{-\infty}^{+\infty} p^{(3)}(v_z)\,F(v_z)\,\mathrm{d}v_z$$
$$= 2N \sum_{\alpha,\beta} \mu_{\beta\alpha} \int_{-\infty}^{+\infty} \rho^{(3)}_{\alpha\beta}(\omega_3, z, t, v_z)\,F(v_z)\,\mathrm{d}v_z\,, \tag{8}$$

where we made use of eq. (4), and where $F(v_z)$ is the distribution function for v_z. For a Maxwell-Boltzmann distribution, we have

$$F(v_z) = (\sqrt{\pi}\,u)^{-1} \exp -(v_z/u)^2\,, \tag{9}$$

with $u = (2k_B T/M)^{1/2}$. Identification between eqs. (3) and (8) then yields the expression for the susceptibility $\chi^{(3)}(\omega_3)$, whose modulus gives the CARS line shape ([4]). We can calculate $\rho^{(3)}_{\alpha\beta}(\omega_3, z, t, v_z)$ either in the laboratory frame or in the molecular frame ; the derivation in the molecular frame is performed in Appendix I for the sake of completeness. In the following, we shall obtain its expression in a straightforward manner by means of the diagrammatic representation.

2.2 DIAGRAMMATIC DERIVATION OF THE DENSITY OPERATOR. — 2.2.1 *Time-ordered diagrams in the space-time domain.* — The density operator at any specified order can be shown to result from a number of contributions ; each of these is associated with a specific time sequence of perturbations to the density operator, or to the ket vector $|\psi\rangle$ and its complex conjugate $\langle\psi|$ (in the pure state case) ; the time-ordering of the perturbations to $|\psi\rangle$ with respect to those to $\langle\psi|$ is of crucial importance in the case of collisional relaxation. It has been demonstrated that each of these elementary time-ordered contributions can be visualized by means of a double-sided Feynman-like diagram, which can be used to write down directly the associated density matrix contribution [12-17]. In the following, we use the conventions of Bordé [14-17] ([5]).

The time evolution of the density matrix is depicted along two parallel vertical bars (one for each subscript of the density matrix) with time increasing upwards. Each interaction with the electromagnetic field is represented by a segment pointing downwards from a vertex if it corresponds to a term oscillating as $e^{-i\omega_j t}$ in the interaction Hamiltonian $V(t)$ (Figs. 2a, 3a), and pointing upwards if the term oscillates as $e^{+i\omega_j t}$ (Figs. 2b, 3b). In addition, when the total field

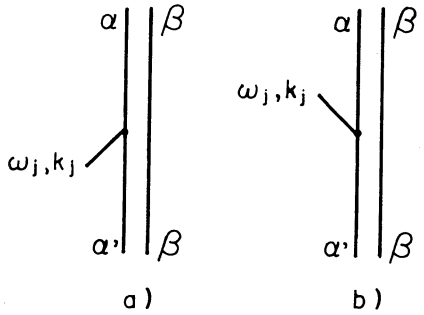

Fig. 2. — Space-time domain diagrams connecting

$$\rho^{(n)}_{\alpha'\beta}(z - v_z\,\tau, t - \tau, v_z) \quad \text{and} \quad \rho^{(n+1)}_{\alpha\beta}(z, t, v_z)$$

in the case of an interaction with field components $e^{-i(\omega_j t - k_j z)}$ (a) and $e^{+i(\omega_j t - k_j z)}$ (b).

([3]) The velocity distribution may either be introduced in $\rho^{(0)}$ or in eq. (4).

([4]) The reasons why we consider the modulus of $\chi^{(3)}(\omega_3)$ and not its square are developed in ref. [2].

([5]) The authors of refs. [12-13] use opposite conventions for drawing the diagrams and calculating the corresponding susceptibility.

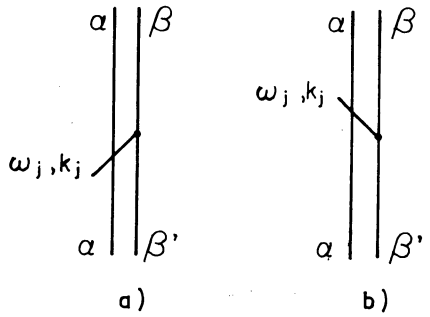

Fig. 3. — Space-time domain diagrams connecting

$\rho^{(n)}_{\alpha\beta'}(z - v_z\,\tau, t - \tau, v_z)$ and $\rho^{(n+1)}_{\alpha\beta}(z, t, v_z)$

in the case of an interaction with field components $e^{-i(\omega_j t - k_j z)}$ (a) and $e^{+i(\omega_j t - k_j z)}$ (b).

is made up of counter-propagating waves, the segment is on the left of the vertical bar if the interaction takes place with the forward propagating wave and on the right otherwise. The vertex is on the left or right hand side vertical bar depending on whether the left or right hand side subscript of $\rho_{\alpha\beta}$ is changed through the interaction. The eigenstates between which the interaction Hamiltonian is operating are indicated below and above each vertex. Starting from a density matrix element $\rho^{(n)}_{\alpha'\beta}$ at a given order n, and assuming that a particular interaction takes place with the electric field component E_j as represented by the one-vertex diagrams of figure 2, we obtain the density matrix element $\rho^{(n+1)}_{\alpha\beta}$ at the following order $n + 1$. We have :

$$\rho^{(n+1)}_{\alpha\beta}(z, t, v_z) = \frac{i}{2\hbar}\,\mu_{\alpha\alpha'}\,E_j\,e^{\pm i\varphi_j}\int_0^\infty d\tau\,e^{-i(\omega_{\alpha\beta} - i\gamma_{\alpha\beta})\tau} \times e^{-i(\pm\omega_j)\,(t-\tau)+i(\pm k_j)(z - v_z\tau)}\,\rho^{(n)}_{\alpha'\beta}(z - v_z\,\tau, t - \tau, v_z) \tag{10}$$

where $\omega_{\alpha\beta} = \omega_\alpha - \omega_\beta$ and $\gamma_{\alpha\beta} = R_{\alpha\beta,\alpha\beta}$ are respectively the frequency and width of the $\alpha \to \beta$ multiphoton transition. In eq. (10) the upper (+) sign is taken if the segment is pointing down from the vertex (Fig. 2a), the lower (−) sign otherwise (Fig. 2b). The same rule is used to obtain $\rho^{(n+1)}_{\alpha\beta}$ from $\rho^{(n)}_{\alpha\beta'}$ (Fig. 3) but with $-\,i\mu_{\beta'\beta}$ in place of $+\,i\mu_{\alpha\alpha'}$ in eq. (10). Finally, when the segment is on the right of the vertical bar (backward propagating wave), the signs in front of k_j must be reversed.

$\rho^{(n+1)}_{\alpha\beta}(z, t, v_z)$ is thus obtained by multiplying $\rho^{(n)}_{\alpha'\beta}(z - v_z\,\tau, t - \tau, v_z)$ (or $\rho^{(n)}_{\alpha\beta'}(z - v_z\,\tau, t - \tau, v_z)$) by the field component at location $z - v_z\,\tau$ and time $t - \tau$ times the propagator of $\rho_{\alpha\beta}$ over the time τ, and by integrating the result over τ.

In CARS, one must combine two vertices at ω_1 and one at ω_2 in order to get the polarization component $P^{(3)}$ (as given in eq. 3); its $e^{-i\omega_3 t}$ dependence implies two segments pointing down from the vertex for the interactions with ω_1 and one pointing up for ω_2. We consider the contribution to this polarization from the set of eigenstates $|\alpha\rangle$, $|\beta\rangle$, $|\gamma\rangle$, $|\delta\rangle$ such that $|\alpha\rangle$ and $|\beta\rangle$ have the same parity and $|\gamma\rangle$, $|\delta\rangle$ have a parity opposite to that of $|\alpha\rangle$ and $|\beta\rangle$. Assuming that γ is connected with α by the first interaction, and δ with α or β by the third interaction, one finds [12, 19] that there are 24 combinations of the vertices giving contributions proportional to $\rho^{(0)}_{\alpha\alpha}$ (there are actually 48 in genuine four wave mixing, i.e. if three distinct frequencies ω_1, ω_1', ω_2 are applied to produce a polarization at $(\omega_1 + \omega_1' - \omega_2)$). The net susceptibility contribution from state $|\alpha\rangle$ is then obtained by summing over all possible states $|\beta\rangle$, $|\gamma\rangle$, $|\delta\rangle$ (including the possibility of two identical states). Finally summation over all possible $|\alpha\rangle$ states must be carried out. Only a few of all these terms have been shown to give appreciable contributions to the CARS susceptibility [2, 11, 12]; they will be considered in turn in the next chapter.

In addition to this space-time domain representation of time-ordered processes, one can also use a representation in energy-momentum space [18, 17]. We shall see now that this latter representation allows one to tell directly if any nonlinear process is subject to Doppler broadening or not.

2.2.2 *Time-ordered energy-momentum diagrams.* — The process of figure 2a can be represented in energy-momentum space by the diagram of figure 4. The molecular momenta and energy levels are given respectively on the horizontal and vertical axes.

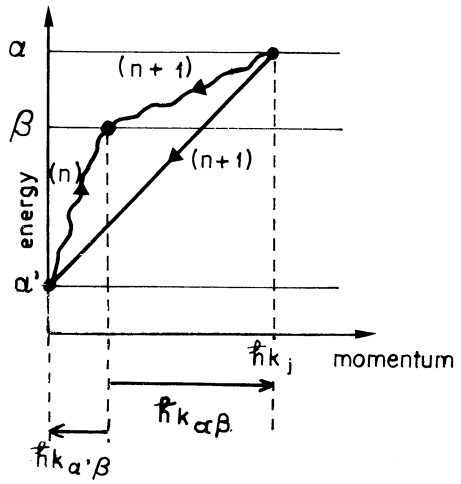

Fig. 4. — Energy-momentum diagram corresponding to the space-time domain diagram of figure 2a. A coherence oriented to the left has a positive wave vector, and *vice versa*. The wave vector of coherence $\alpha\beta$ is thus : $\mathbf{k}_{\alpha\beta} = \mathbf{k}_j - \mathbf{k}_{\alpha'\beta}$.

Stars and wavy lines represent respectively the populations and coherences which build up through successive interactions; for instance, one starts in figure 4 with a coherence $\alpha' \beta$ labelled n (for the order of perturbation) and ends up after one interaction with a coherence $\alpha\beta$ labelled $n + 1$. Field interactions are represented by oriented straight lines going from one energy-momentum state to the next. Their orientation indicates which matrix element of $V(t)$ must be taken for the particular transition ($\mu_{\alpha\alpha'}$ in the case of figure 4). Finally, the transition is labelled according to its rank in the time sequence of interactions, i.e. $n + 1$ in figure 4. The slope will be positive for interaction with a forward propagating wave, negative otherwise.

The coherence $\alpha\beta$ possesses a wavector $\mathbf{k}_{\alpha\beta}$ which satisfies the relationship

$$\mathbf{k}_{\alpha\beta} = \sum_{j=1}^{n+1} \mathbf{k}_j \qquad (11)$$

where the summation is taken over the complete set of $n + 1$ waves which interact with the molecule to establish the coherence $\alpha\beta$. It has been established [8, 18, 21, 22] that the $\alpha \rightarrow \beta$ transition under probe will not be subject to Doppler broadening if the condition

$$\mathbf{k}_{\alpha\beta} = 0 \qquad (12)$$

is satisfied, or, in other words, if the coherence is vertical in figure 4. Then all molecules participate equally and we have a true Doppler-free process. This is the case of two-photon absorption lines as well as three-photon absorption lines which are Doppler-free under certain experimental conditions [21, 22]; for such processes, the relationship (12) had been formulated slightly differently by Cagnac and coworkers as *the sum of momenta of absorbed and emitted photons is zero* [21, 22].

We shall see in the next section that the Raman coherence ab never satisfies condition (12) in CARS and other Raman mixing processes such as CSRS or SRS, since $\mathbf{k}_{ab} = \mathbf{k}_1 - \mathbf{k}_2$ is always non zero. For forward mixing, $|\mathbf{k}_{ab}|$ is minimal and we have the residual broadening presented in the introduction. Still, it is possible for such a transition to result in a Doppler-free signal if it has a level in common with another resonant transition. This is because a specific velocity group, and one only, makes the two coupled transitions simultaneously resonant, resulting in a Doppler-free signal superimposed on the smaller Doppler-broadened signal contributed by all the other velocity groups. Then not all molecules participate, contrary to the true Doppler-free case. This occurs in saturated absorption as well as in a number of time-ordered terms in CARS, CSRS and SRS at electronic resonance; however additional conditions have to be met and not all terms in the CARS susceptibility satisfy them, as will be seen in the next section. We call the corresponding lines *selectively Doppler-free.*

3. **Application to CARS.** — 3.1 CHOICE AND DERIVATION OF THE RELEVANT SUSCEPTIBILITY TERMS. — The discussion of CARS is not simple. Each term in the susceptibility calculated following the rules given in 2.2.1 has three characteristic energy denominators, and hence exhibits distinct spectral properties. We recall that CARS spectroscopy is performed by tuning $\omega_1 - \omega_2$ across the frequency ω_{ba} of a given Raman transition. Further, resonant CARS is obtained when, in addition, one or more of the three frequencies ω_1, ω_2 or ω_3 is close to a one-photon transition frequency pertaining to states $|a\rangle$ or $|b\rangle$ (Fig. 1); the problem is then to calculate the net CARS susceptibility of a four-level system. For the set of energy levels of interest a, b, n, n' such as that of figure 1, one calculates 24 terms proportional to $\rho_{aa}^{(0)}$ in the CARS susceptibility by taking $|n\rangle$ for the first transition; another 24 terms are obtained by taking $|n'\rangle$ first, plus 24 using $|n\rangle$ twice and not $|n'\rangle$ and 24 using $|n'\rangle$ twice, for a total of 96 terms. Another 96 combinations are calculated by replacing $|b\rangle$ by $|a\rangle$. There are as many (192) contributions proportional to $\rho_{bb}^{(0)}$. These exhaust the entire susceptibility from the four levels a, b, n, n', of figure 1, assuming that levels n and n' are not initially populated.

Off electronic resonance, one finds 32 terms among the 192 terms calculated above which possess the Raman resonance $\omega_{ba} - \omega_1 + \omega_2 = 0$ (16 are proportional to $\rho_{aa}^{(0)}$ and the others to $\rho_{bb}^{(0)}$). It is sufficient to consider only the 8 terms calculated using $|n\rangle$ for the first transition if a summation is performed over all possible levels n and n' without any additional condition on their energy order (including $n = n'$); the diagrammatic representation of these 8 terms in the space-time domain is shown in figure 5.

On resonance, the contributions of figures 5a, 5e become very large, and the six other contributions can be neglected since they possess at least one anti-resonant one-photon denominator. In addition, one must also take into account terms possessing the two-photon resonance $\omega_{n'n} - \omega_1 + \omega_2 = 0$ where $\omega_{n'n}$ is a vibrational frequency of the excited electronic state.

Some of them are represented in figure 6; in particular diagrams 6c and 6d depict two terms which are studied in ref. [12], where they are called *corrective* terms because they do not possess the Raman resonance. As a matter of fact, the strongest features in the resonant CARS spectrum result from these *corrective* terms as well as from the Raman resonant terms, depending on the relative spectral positions of ω_1, ω_2, ω_3 in the absorption spectrum. All the other terms constitute what is called the non-resonant part of the susceptibility, which is small and has little influence on the line profile in a pure gas (whether on- or off-resonance). We shall see that, among the Raman resonant terms, some can be selectively Doppler-free while the others are not; furthermore, some of the *corrective* terms are also Doppler-free. Since the terms which are Doppler-free produce spectral fea-

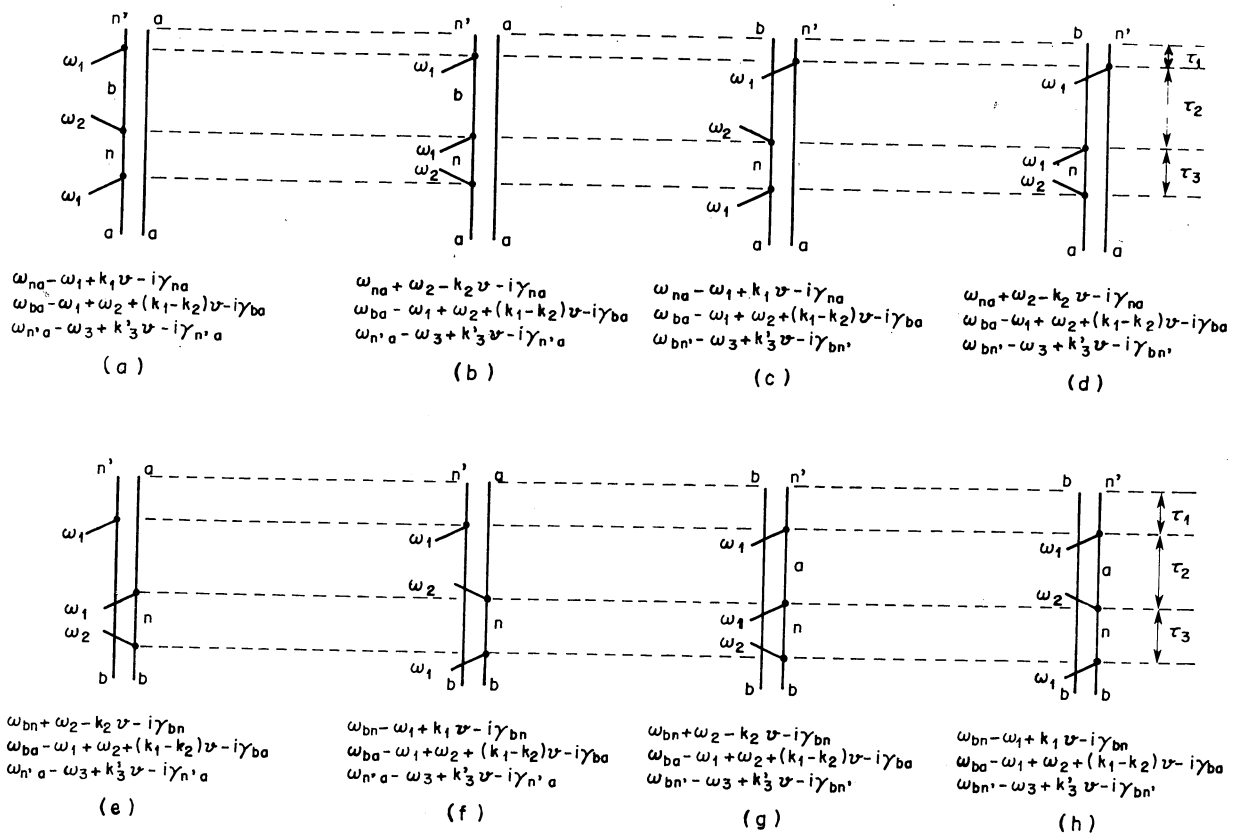

Fig. 5. — Diagrammatic representation in the space-time domain of the Raman resonant contributions to $\chi^{(3)}(\omega_3)$ calculated by taking n first : a-d, contributions proportional to $\rho^{(0)}_{aa}$; e-h, contributions proportional to $\rho^{(0)}_{bb}$. The corresponding three energy denominators are indicated under each diagram. The other Raman resonant contributions are easily obtained by (1) interchanging n and n', or (2) replacing n' by n, or (3) replacing n by n', in each of these diagrams.

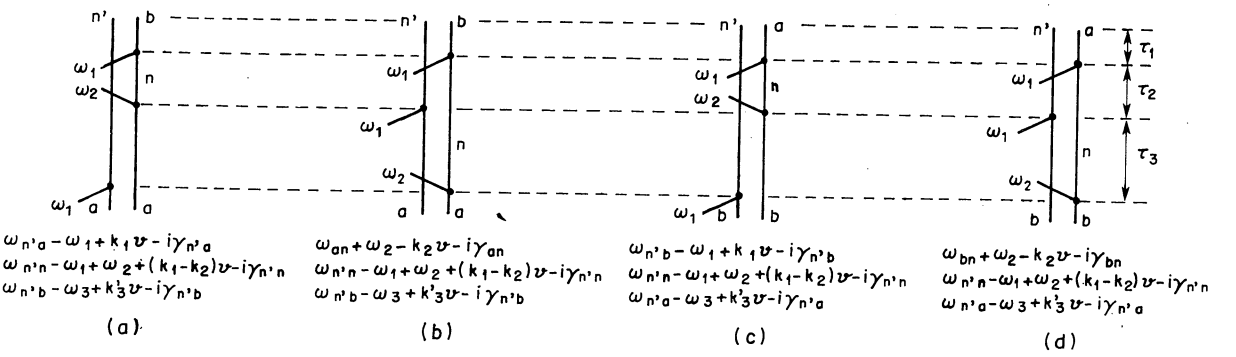

Fig. 6. — Diagrammatic representation of four contributions to $\chi^{(3)}(\omega_4)$ having the resonant denominator $(\omega_{n'n} - \omega_1 + \omega_2)$. In this figure n' and n are imposed by the resonance condition $\omega_{n'n} - \omega_1 + \omega_2 = 0$ (similar to the condition on a and b for figure 5). The main diagrams are (a) and (b) ; one should also consider all diagrams derived from these by (1) interchanging a and b, or (2) replacing a by b, or (3) replacing b by a. As an example, diagrams (c) and (d) are obtained from diagrams (a) and (b) by interchanging a and b.

tures which are inherently stronger and narrower, we have the important consequence that the resonant CARS spectral content at low pressure can be quite different from that at high pressure. There are indeed terms (not shown in Figs. 5, 6) which were not considered in the collision broadening limit [12] and which can become important at low pressure if they are selectively Doppler-free (such as Raman anti-resonant terms possessing the denominator

$$\omega_{ba} + \omega_1 - \omega_2 + i\gamma_{ba}) .$$

In this paper, we shall restrict the discussion to the terms represented in figures 5 and 6. To illustrate the use of the diagrammatic representation, we shall now write the expression for the term associated with diagram (a) of figure 5 using eq. (10) :

$$\rho^{(3)}_{n'a}(\omega_3, z, t, v_z) = i\frac{\mu_{n'b} E_1 e^{i\varphi_1}}{2\hbar}\int_0^\infty d\tau_1 e^{-i(\omega_{n'a}-i\gamma_{n'a})\tau_1} e^{-i\omega_1(t-\tau_1)} \times$$
$$\times e^{+ik_1(z-v_z\tau_1)}\frac{i\mu_{bn} E_2 e^{-i\varphi_2}}{2\hbar}\int_0^\infty d\tau_2 e^{-i(\omega_{ba}-i\gamma_{ba})\tau_2} e^{+i\omega_2(t-\tau_1-\tau_2)} e^{-ik_2(z-v_z(\tau_1+\tau_2))}$$
$$\times \frac{i\mu_{na} E_1 e^{i\varphi_1}}{2\hbar}\int_0^\infty d\tau_3 e^{-i(\omega_{na}-i\gamma_{na})\tau_3} e^{-i\omega_1(t-\tau_1-\tau_2-\tau_3)} e^{+ik_1(z-v_z(\tau_1+\tau_2+\tau_3))} \times \rho^{(0)}_{aa} . \quad (13)$$

Integrating over τ_1, τ_2, τ_3 and using eqs. (3) and (8) we obtain :

$$\chi^{(3)}_{5a}(\omega_3) = \hbar^{-3} N\rho^{(0)}_{aa}\mu_{an'}\mu_{n'b}\mu_{bn}\mu_{na}\int_{-\infty}^{+\infty} dv_z F(v_z) \times$$
$$\times \frac{1}{\omega_{n'a} - \omega_3 - i\gamma_{n'a} + k'_3 v_z} \times \frac{1}{\omega_{ba} - \omega_1 + \omega_2 - i\gamma_{ba} + (k_1 - k_2) v_z} \times \frac{1}{\omega_{na} - \omega_1 - i\gamma_{na} + k_1 v_z} \quad (14)$$

where the Doppler shifts on field frequencies appear explicitely.

The other terms can be calculated in a similar way. In most cases, a resonant CARS line is due to a double or triple resonance occurring in one single contribution to $\chi^{(3)}(\omega_3)$, and the integration over v_z has to be done in each specific case. We shall consider the different cases in turn, starting with the simpler case of off-resonance CARS.

3.2 OFF-RESONANCE CARS. — We consider the above mentioned eight terms possessing the Raman resonant denominator (Fig. 5). In these contributions the frequency and v_z dependence of the one-photon denominators may be neglected over the tuning range corresponding to the Raman resonance ; we then arrive at the following expression for the resonant part χ_R of $\chi^{(3)}(\omega_3)$:

$$\chi_R = N\frac{\rho^{(0)}_{aa} - \rho^{(0)}_{bb}}{\hbar^3} K \times \int_{-\infty}^{+\infty} dv_z \frac{F(v_z)}{\omega_{ba} - \omega_1 + \omega_2 - i\gamma_{ba} + (k_1 - k_2) v_z}, \quad (15)$$

with :

$$K = \sum_{n,n'}\left(\frac{\mu_{an'}\mu_{n'b}}{\omega_{n'a} - \omega_3} + \frac{\mu_{an'}\mu_{n'b}}{\omega_{n'b} + \omega_3}\right)\left(\frac{\mu_{bn}\mu_{na}}{\omega_{na} - \omega_1} + \frac{\mu_{bn}\mu_{na}}{\omega_{na} + \omega_2}\right).$$

The integration over v_z in (15) is the convolution product of $F(v_z)$, which is a Gaussian, with a complex Lorentzian ; this product can be expressed in terms of the complex error function $w(\zeta)$ [23] such that :

$$\int_{-\infty}^{+\infty} d\theta \frac{e^{-\theta^2}}{\eta - i(\xi \pm \theta)} = \pi w(\zeta) \quad (16)$$

with $\zeta = \xi + i\eta$ and $\theta = v_z/u$.

From (15) and (16), one obtains :

$$\chi_R = N\frac{\rho^{(0)}_{aa} - \rho^{(0)}_{bb}}{\hbar^3} \times K \times \frac{\sqrt{\pi}}{(k_1 - k_2) u} i w^*(\zeta_{ba}), \quad (17)$$

with ([6])

$$\zeta_{ba} = \frac{\omega_{ba} - \omega_1 + \omega_2 + i\gamma_{ba}}{(k_1 - k_2) u} = \xi_{ba} + i\eta_{ba} .$$

The CARS line profile is thus given by $| w^*(\zeta_{ba}) |$ *versus* $\omega_1 - \omega_2$, which is tabulated or can be obtained numerically. Figure 7 shows a numerical calculation of $| w^*(\zeta_{ba}) |$ *versus* ξ_{ba} in the limit of zero homogeneous linewidth ($\eta_{ba} = 0$) ; also shown in the figure are the real and imaginary parts of $w(\zeta_{ba})$. The real part is purely Gaussian with full width at half maximum (FWHM) $\Delta\nu_D = \omega_{ba} u \sqrt{\ln 2}/\pi c$. Let us note here that this Gaussian is precisely the profile of the lines obtained in forward spontaneous Raman scattering. The CARS lines are not Gaussian because of the additional dispersive part of χ_R [9] ; from figure 7, the FWHM is about 1.78 $\Delta\nu_D$.

3.3 RESONANT CARS. — Quite generally, the stronger features in resonant CARS spectra are provided by a double resonance (in some cases, a triple resonance) occurring in one of the contributions depicted in figures 5a, 5e and 6. Depending on the contribution which is being probed, the line profile is best interpreted by fixing either ω_1 or ω_2 and by varying the other, so that one of the energy denominators remains constant during the spectral scan while the other two vary.

([6]) If the opposite sign is chosen for ξ_{ba}, w^* in eq. (17) is replaced by w since $w^*(\zeta) = w(-\zeta^*)$.

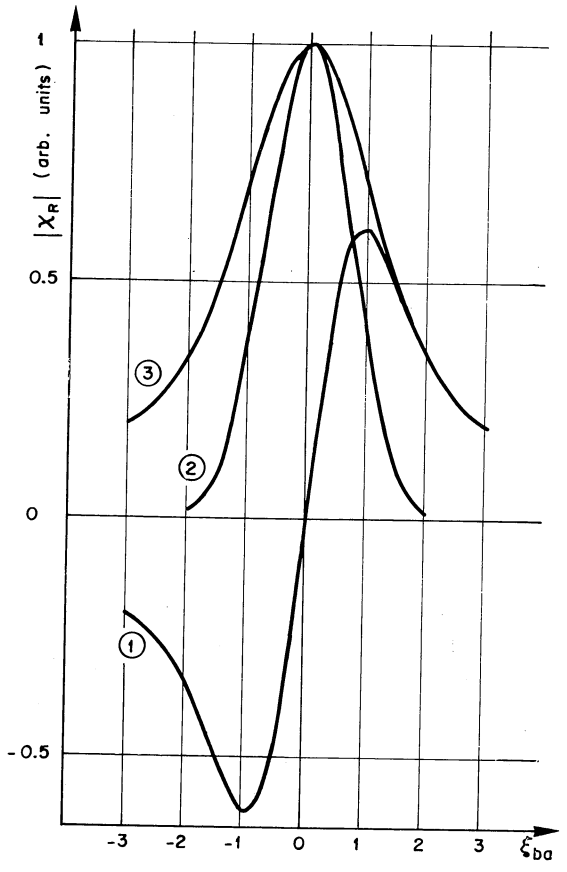

Fig. 7. — Off resonance CARS line shape in the Doppler limit. (1) plot of the imaginary, dispersive, part of $w(\xi_{ba})$ *versus* ξ_{ba}; (2) plot of the Gaussian real part of $w(\xi_{ba})$; (3) plot of $|\, w^*(\xi_{ba})\,|$.

3.3.1 *Term depicted in figure* 5a. — It has been shown previously that when ω_1 is set near a one-photon absorption ω_{na} of the molecules and ω_2 is varied about $\omega_1 - \omega_{ba}$, three families of lines are found in the CARS spectrum [2, 11, 12]. They correspond to the three possibilities of double resonance in the main susceptibility term $\chi^{(3)}_{5a}(\omega_3)$ (Fig. 5a) which is proportional to population factor $\rho^{(0)}_{aa}$ and whose expression is given by eq. (14). These double resonances have been labelled

$$(\omega_1 = \omega_{na},\ \omega_1 - \omega_2 = \omega_{ba}),$$
$$(\omega_1 = \omega_{na},\ \omega_3 = \omega_{n'a}),$$
$$(\omega_1 - \omega_2 = \omega_{ba},\ \omega_3 = \omega_{n'a}),$$

and have been called respectively laser-enhanced Raman lines, electronic lines and anti-Stokes-enhanced Raman lines. Note that the third type of resonance implies $\omega_1 = \omega_{n'b}$, and therefore that the set of eigenstates $|\, a\,\rangle$, $|\, b\,\rangle$, $|\, n\,\rangle$, $|\, n'\,\rangle$ which gives the largest contribution to the susceptibility is generally different from that of the first two types.

For the laser-enhanced Raman lines, the first denominator in (14) is large enough for its v_z dependence to be neglected, and we obtain, using $\dfrac{1}{ab} = \dfrac{1}{b-a}\left(\dfrac{1}{a} - \dfrac{1}{b}\right)$:

$$\chi^{(3)}_{5a}(\omega_3) = N\rho^{(0)}_{aa}\,\frac{\mu_{an'}\,\mu_{n'b}\,\mu_{bn}\,\mu_{na}}{\hbar^3(\omega_{n'a} - \omega_3 - i\gamma_{n'a})} \times \frac{1}{k_1(k_1 - k_2)\,u^2} \times \frac{1}{\zeta^*_{ba} - \zeta^*_{na}} \times$$
$$\times \int_{-\infty}^{+\infty} \mathrm{d}\theta\, \frac{\exp - \theta^2}{\sqrt{\pi}} \left(\frac{1}{\zeta^*_{na} + \theta} - \frac{1}{\zeta^*_{ba} + \theta}\right) \qquad (18)$$

with ζ_{ba} as defined for eq. (17) and

$$\zeta_{na} = \frac{\omega_{na} - \omega_1 + i\gamma_{na}}{k_1\,u} = \xi_{na} + i\eta_{na}\,.$$

The integral in (18) is the sum of two convolution products which can be expressed in terms of two complex error functions (eq. (16)) :

$$\chi^{(3)}_{5a}(\omega_3) = N\rho^{(0)}_{aa}\,\frac{\mu_{an'}\,\mu_{n'b}\,\mu_{bn}\,\mu_{na}}{\hbar^3(\omega_{n'a} - \omega_3 - i\gamma_{n'a})} \times \frac{(-i\sqrt{\pi})}{k_1(k_1 - k_2)\,u^2} \times \frac{w^*(\zeta_{ba}) - w^*(\zeta_{na})}{\zeta^*_{ba} - \zeta^*_{na}}\,. \qquad (19)$$

Eq. (19) is evaluated numerically ; for the singularity $\zeta_{ba} = \zeta_{na}$ we use the following formula :

$$\lim_{\zeta_{ba} \to \zeta_{na}} \frac{w^*(\zeta_{ba}) - w^*(\zeta_{na})}{\zeta^*_{ba} - \zeta^*_{na}} = w'^*(\zeta_{ba}) = -2\,i/\sqrt{\pi} - 2\,\zeta^*_{ba}\,w^*(\zeta_{ba})\,.$$

Plots of $\left|\dfrac{w^*(\zeta_{ba}) - w^*(\zeta_{na})}{\zeta^*_{ba} - \zeta^*_{na}}\right|$ *versus* ζ_{ba} for detunings $(\omega_{na} - \omega_1)/2\,\pi$ going from 0, i.e. $\xi_{na} = 0$, to $2(\omega_{na}/\omega_{ba})\,\Delta\nu_D$, i.e. $\xi_{na} = 4\sqrt{\ln 2}$, are shown in figure 8 ; these curves were obtained for an homogeneous width $\gamma = \gamma_{na} = \gamma_{ba} = \pi\,\Delta\nu_D \times 10^{-4}$. The velocity group which makes the two coupled transitions simultaneously

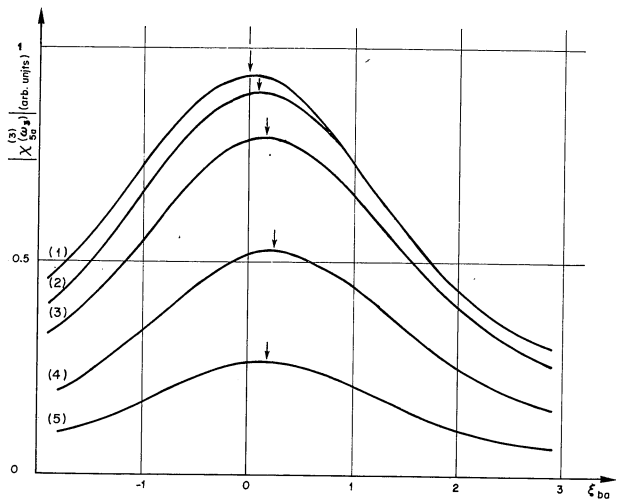

Fig. 8. — Laser-enhanced Raman line associated with diagram (a) of figure 5. We took $\gamma = \gamma_{na} = \gamma_{ba} = \pi \Delta\nu_D \times 10^{-4}$ and the following set of values for ξ_{na} : 0 (curve 1), $\sqrt{\ln 2}/2$ (2), $\sqrt{\ln 2}$ (3), $2\sqrt{\ln 2}$ (4), $4\sqrt{\ln 2}$ (5). We measure from the graphs a FWHM of 2.21 $\Delta\nu_D$ (curve 1), 2.30 $\Delta\nu_D$ (2), 2.40 $\Delta\nu_D$ (3), 2.33 $\Delta\nu_D$ (4), 2.04 $\Delta\nu_D$ (5). The arrows indicate the positions of the line maxima.

resonant is here $v_0 = -(\omega_{na} - \omega_1)/k_1 = -\xi_{na}\, u$. The spectral contribution of molecules with velocity v_0 is located at $\omega_1 - \omega_2 = \omega_{ba} + (k_1 - k_2)\, v_0$ or, equivalently, at $\xi_{ba} = \xi_{na}$. We can see in figure 8 that there is no discernible resonance at this position and that the CARS line is clearly subject to Doppler broadening ; the FWHM is more than twice that for forward Raman scattering.

The line maximum is only slightly shifted from $\xi_{ba} = 0$ towards $\xi_{ba} = \xi_{na}$, as a result of the stronger, although not dominant, contribution of the velocity group v_0.

Quite similarly, the integration of (14) leads to the following expression for the electronic line ($\omega_1 \simeq \omega_{na}$, $\omega_3 \simeq \omega_{n'a}$) :

$$\chi^{(3)}_{5a}(\omega_3) = N\rho^{(0)}_{aa} \frac{\mu_{an'}\, \mu_{n'b}\, \mu_{bn}\, \mu_{na}}{\hbar^3(\omega_{ba} - \omega_1 + \omega_2 - i\gamma_{ba})} \times \frac{(-i\sqrt{\pi})}{k_1\, k'_3\, u^2} \times \frac{w^*(\zeta_{n'a}) - w^*(\zeta_{na})}{\zeta^*_{n'a} - \zeta^*_{na}}, \tag{20}$$

with

$$\zeta_{n'a} = (\omega_{n'a} - \omega_3 + i\gamma_{n'a})/k'_3\, u = \xi_{n'a} + i\eta_{n'a}\,.$$

The line profile is given by the plot of $\left| \frac{w^*(\zeta_{n'a}) - w^*(\zeta_{na})}{\zeta^*_{n'a} - \zeta^*_{na}} \right|$ *versus* $\xi_{n'a}$ and is identical to those of figure 8 with reduced variable ζ_{ba} replaced by $\zeta_{n'a}$. As a consequence, the width of the electronic line is of the order of the full Doppler width of the one-photon electronic absorption line. It is larger than that of the laser-enhanced Raman line by a factor $k'_3/(k_1 - k_2)$. We also note by comparing (19) and (20) that the maximum intensity of the electronic line is smaller than that of the laser-enhanced Raman line by the same factor.

For the anti-Stokes-enhanced Raman lines one obtains from (14) :

$$\chi^{(3)}_{5a}(\omega_3) = N\rho^{(0)}_{aa} \frac{\mu_{an'}\, \mu_{n'b}\, \mu_{bn}\, \mu_{na}}{\hbar^3(\omega_{na} - \omega_1 - i\gamma_{na})} \times \frac{(-i\sqrt{\pi})}{(k_1 - k_2)\, k'_3\, u^2} \times \frac{w^*(\zeta_{ba}) - w^*(\zeta_{n'a})}{\zeta^*_{ba} - \zeta^*_{n'a}}, \tag{21}$$

here the line shape is expected to be more complex than in the two above cases because both ζ_{ba} and $\zeta_{n'a}$ vary during the spectral scan. Indeed, in the limit of pure collision broadening this type of line shows two maxima, i.e. one at $\omega_1 - \omega_2 = \omega_{ba}$ and the other at $\omega_1 - \omega_2 = \omega_{ba} - \omega_1 + \omega_{n'b}$ (i.e. $\omega_3 = \omega_{n'a}$) ; when $\omega_1 = \omega_{n'b}$ the two maxima merge resulting in a stronger and narrower line.

Plots of $\left| \frac{w^*(\zeta_{ba}) - w^*(\zeta_{n'a})}{\zeta^*_{ba} - \zeta^*_{n'a}} \right|$ in the Doppler limit ($\eta_{n'a} = \eta_{ba} = 0$) are shown in figure 9. In figure 9a, which corresponds to a situation of experimental interest, the line shape has only one maximum very close to $\omega_1 - \omega_2 = \omega_{ba}$. The other maximum, which we expected to be at $\xi_{ba} = -(\omega_{n'b} - \omega_1)/(k_1 - k_2)\, u = -3.3$, is too weak to be seen. This is due to the Doppler broadening affecting this type of line. The broadening of the component at $\xi_{ba} = 0$ (Raman resonance) is of the order of 2 $\Delta\nu_D$ while that of the other component (electronic resonance $\omega_3 = \omega_{n'a}$) is $k'_3/(k_1 - k_2)$ times larger ; as a result the intensity of the electronic component is a factor of $k'_3/(k_1 - k_2)$ times lower than that of the Raman one, i.e. 14.3 in the case of figure 9a. In figure 9b we have

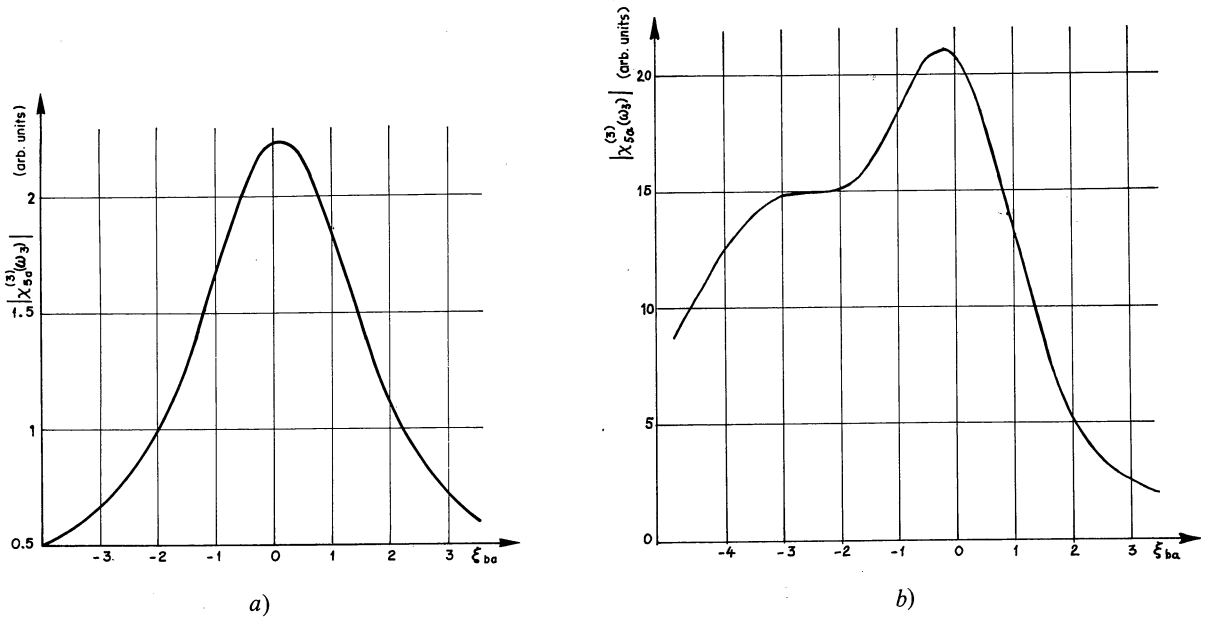

a) b)

Fig. 9. — Anti-Stokes-enhanced Raman lines associated with figure 5a, using $\gamma_{n'a} = \gamma_{ba} = 0$. (a) We took $\omega_{n'b} - \omega_1/2\pi = 2\,\Delta\nu_D$. We also took values of ω_1 and ω_{ba} corresponding to the iodine experiment of ref. [11] : $\omega_1 = 16\,955.5\ \text{cm}^{-1}$, $\omega_{ba} = 1\,260\ \text{cm}^{-1}$ which gives $k'_3/(k_1 - k_2) = 14.3$. We measure for the FWHM $2.28\,\Delta\nu_D$. (b) Same CARS line as in figure 9a, but taking : $(\omega_{n'b} - \omega_1)/2\pi = 2.25\,\Delta\nu_D$, $\omega_1 = 16\,955.5\ \text{cm}^{-1}$, $\omega_{ba} = 33\,911\ \text{cm}^{-1}$ to show the splitting discussed in the text.

taken another set of parameters so that this latter factor is now 1.5 ; the splitting of the line into its Raman and electronic parts is then clearly visible.

To be complete, we shall now calculate $\chi^{(3)}_{5a}(\omega_3)$ in the case of a triple resonance. Using

$$\frac{1}{abc} = \frac{1}{b-a}\left(\frac{1}{ac} - \frac{1}{bc}\right) = \frac{1}{(b-a)(c-a)a} + \frac{1}{(a-b)(c-b)b} + \frac{1}{(c-a)(c-b)c},$$

we obtain from (14) :

$$\chi^{(3)}_{5a}(\omega_3) = N\rho^{(0)}_{aa}\frac{\mu_{an'}\,\mu_{n'b}\,\mu_{bn}\,\mu_{na}}{\hbar^3\,k_1(k_1-k_2)\,k'_3}\left(\frac{i\sqrt{\pi}}{u^3}\right)\times$$
$$\times\left(\frac{w^*(\zeta_{na})}{(\zeta^*_{ba}-\zeta^*_{na})(\zeta^*_{n'a}-\zeta^*_{na})} + \frac{w^*(\zeta_{ba})}{(\zeta^*_{na}-\zeta^*_{ba})(\zeta^*_{n'a}-\zeta^*_{ba})} + \frac{w^*(\zeta_{n'a})}{(\zeta^*_{n'a}-\zeta^*_{na})(\zeta^*_{n'a}-\zeta^*_{ba})}\right). \quad (22)$$

This function is also obtained numerically. For the limiting case $\zeta_{na} = \zeta_{ba} = \zeta_{n'a}$, it can be expressed in terms of the second derivative $w''(\zeta)$ of the complex error function :

$$\chi^{(3)}_{5a}(\omega_3) = -\,N\rho^{(0)}_{aa}\frac{\mu_{an'}\,\mu_{n'b}\,\mu_{bn}\,\mu_{na}}{\hbar^3\,k_1(k_1-k_2)\,k'_3}\times\frac{i\sqrt{\pi}}{u^3}\times\frac{w''^*(\zeta_{n'a})}{2}. \quad (23)$$

Let us note here that when one of the reduced variables $|\,\zeta_{n'a}\,|$ or $|\,\zeta_{ba}\,|$ or $|\,\zeta_{na}\,|$ is large with respect to its associated Doppler broadening parameter (respectively $k'_3\,u$, $k_1\,u$, $(k_1 - k_2)\,u$), eq. (22) transforms respectively into eqs. (19), (20) or (21) obtained above for the 3 types of double resonance. For instance, if we have

$$|\,\zeta_{n'a}\,| \gg k'_3\,u \gtrsim |\,\zeta_{ba}\,|,\ |\,\zeta_{na}\,|$$

we obtain from (22) :

$$\chi^{(3)}_{5a}(\omega_3) \to N\rho^{(0)}_{aa}\frac{\mu_{an'}\,\mu_{n'b}\,\mu_{bn}\,\mu_{na}}{\hbar^3(k_1-k_2)\,k_1\,k'_3\,u^3}(i\sqrt{\pi})\left(\frac{w^*(\zeta_{n'a})}{(\zeta^*_{n'a})^2} + \frac{w^*(\zeta_{na})}{(\zeta^*_{ba}-\zeta^*_{na})\,\zeta^*_{n'a}} - \frac{w^*(\zeta_{ba})}{(\zeta^*_{ba}-\zeta^*_{na})\,\zeta^*_{n'a}}\right) \quad (24)$$

which becomes using $\lim_{|\zeta|\to\infty}\dfrac{w^*(\zeta)}{\zeta^2} = 0$:

$$\chi^{(3)}_{5a}(\omega_3) = N\rho^{(0)}_{aa}\ \frac{\mu_{an'}\,\mu_{n'b}\,\mu_{bn}\,\mu_{na}}{\hbar^3(k_1-k_2)\,k_1\,u^2}\left(\frac{-\,i\sqrt{\pi}}{\omega_{n'a}-\omega_3-i\gamma_{n'a}}\right)\frac{w^*(\zeta_{ba}) - w^*(\zeta_{na})}{\zeta^*_{ba}-\zeta^*_{na}}$$

which is identical to eq. (19) obtained previously for the laser-enhanced Raman line. The plots of $|\chi^{(3)}_{5a}(\omega_3)|$ as given in eq. (22) are shown in figure 10 ; the FWHM is about 2.6 $\Delta\nu_D$ for the two cases shown and these triple resonance lines are clearly subject to Doppler broadening. We note also that the line profile, which has two maxima in the collisional broadening limit for the same reason as for the anti-Stokes-enhanced Raman line, has here also only one maximum near $\xi_{ba} = 0$.

These results show that the existence of one specific velocity group v_0 giving a larger signal than the other groups is not a sufficient condition for a nonlinear process to be Doppler-free. The pertinent question is as follows : is the signal due to velocity group v_0 and nearby velocity groups within the homogeneous width really overwhelming or not ?

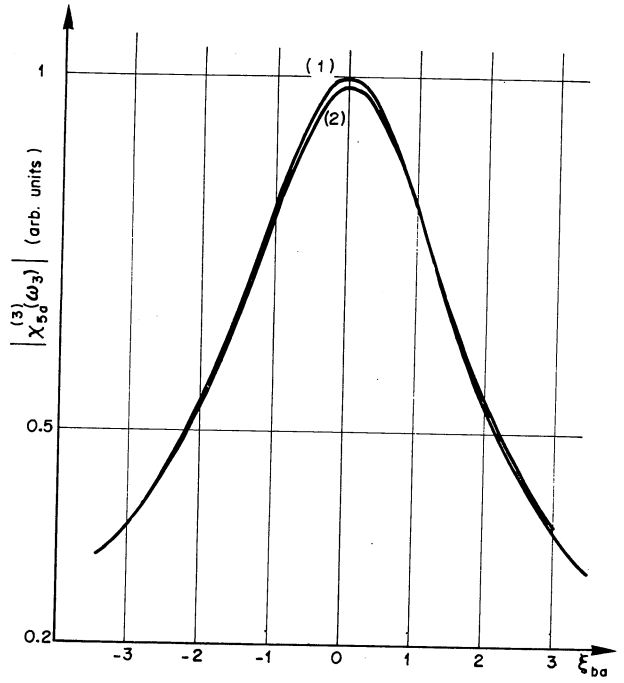

Fig. 10. — Triple resonance associated with figure 5a in the Doppler limit ($\eta_{na} = \eta_{ba} = \eta_{n'a} = 0$), with $\xi_{na} = 0$ and with $\omega_{n'b} - \omega_1 = 0$ (curve 1), $(\omega_{n'b} - \omega_1)/2\pi = 2\,\Delta\nu_D$ (curve 2). We measure for the FWHM 2.64 $\Delta\nu_D$ (1) and 2.57 $\Delta\nu_D$ (2).

3.3.2 *Condition for a multiple resonance line to be Doppler-free.* — Whether the contributions of the velocity groups add in phase or not in the susceptibility will give the answer to this question. Quite generally, we have for the contribution to $\chi^{(3)}(\omega_3)$ of a given time-ordered process l :

$$\chi^{(3)}_l(\omega_3) = \int_{-\infty}^{+\infty} dv_z\, F(v_z) \iiint_0^{+\infty} d\tau_1\, d\tau_2\, d\tau_3\, f(\tau_1, \tau_2, \tau_3)\, e^{i\varphi(v_z,\tau_1,\tau_2,\tau_3)}$$

where $\varphi(v_z, \tau_1, \tau_2, \tau_3)$ is the v_z dependent part of the phase of the integrand ; this phase is a linear combination of the time intervals τ_i between two successive interactions, the coefficients of which are the $k^{(i)}_{\alpha\beta}$ of the coherences established during these time intervals, *viz.*

$$\varphi(v_z, \tau_1, \tau_2, \tau_3) = \sum_{i=1}^{3} k^{(i)}_{\alpha\beta}\, \tau_i\, v_z\,, \tag{25}$$

where, if a given interaction (i) is highly nonresonant, the effective time τ_i for which one has a non zero contribution to the integral is very short so that the contribution from τ_i to eq. (25) can be disregarded. $\varphi(v_z, \tau_1, \tau_2, \tau_3)$ is the phase of the contribution of velocity group v_z relative to that of the contribution of velocity 0 for each set of time intervals (τ_1, τ_2, τ_3). One simple way to tell whether the velocity group centred at v_0 gives an overwhelming contribution or not is to take the slowly varying function outside the v_z integral and replace it by $F(v_0) = F$:

$$\chi^{(3)}_l(\omega_3) = F \int_{-\infty}^{+\infty} dv_z \iiint_0^{+\infty} d\tau_1\, d\tau_2\, d\tau_3\, f(\tau_1, \tau_2, \tau_3)\, e^{i\varphi(v_z,\tau_1,\tau_2,\tau_3)}\,. \tag{26}$$

In eq. (26) the integration over v_z can be performed either before or after that over the τ's. We shall present these two derivations in turn.

a) *Integration over v_z performed first.* — Combining eqs. (25), (26) we obtain :

$$\chi_l^{(3)}(\omega_3) = 2\,\pi F \iiint \mathrm{d}\tau_1\,\mathrm{d}\tau_2\,\mathrm{d}\tau_3\, f(\tau_1, \tau_2, \tau_3)\,\delta\left(\sum_{i=1}^{3} k_{\alpha\beta}^{(i)}\,\tau_i\right). \tag{27}$$

The susceptibility $\chi_l^{(3)}(\omega_3)$ can be non zero only if sets of time intervals such that

$$\sum_{i=1}^{3} k_{\alpha\beta}^{(i)}\,\tau_i = 0$$

can be found. For such sets, the velocity groups contribute in phase to $\chi_l^{(3)}(\omega_3)$ since $\varphi(v_z, \tau_1, \tau_2, \tau_3) = 0$, and therefore interfere constructively with the dominant contribution of v_0, resulting in a Doppler-free line ; on the other hand, if no such set of time intervals can be found, we have $\chi_l^{(3)}(\omega_3) = 0$, which means that taking F out of the integral was not justified and therefore that the line has the full Doppler width. Let us note finally that $\varphi(v_z, \tau_1, \tau_2, \tau_3)$ can be readily written down from the space-time domain diagrams using the rule given in eq. (10), so that it is easy to determine whether a time-ordered process is Doppler-free or not without machine calculation. In the case of the above-mentioned laser-enhanced Raman lines, $\varphi(v_z, \tau_1, \tau_2, \tau_3)$ is obtained from eq. (13) ; we have $\varphi(v_z, \tau_2, \tau_3) = (k_1\,\tau_3 + (k_1 - k_2)\,\tau_2)\,v_z$ where time τ_1 needs not be considered because the detuning $(\omega_{n'a} - \omega_3)$ is very large, as was stated in the discussion of eq. (25).

Since both k_1 and $k_1 - k_2$ are positive, $\varphi(v_z, \tau_3, \tau_2)$ cannot be zero, which confirms that the line is Doppler broadened.

b) *Integration over the τ's performed first.* — Integrating eq. (26) over the τ's leads to :

$$\chi_l^{(3)}(\omega_3) = F \int_{-\infty}^{+\infty} \mathrm{d}v_z\, g(v_z) \tag{28}$$

where $g(v_z)$ is the product of three complex Lorentzians (see for instance eq. (14) in the case of figure 5a). The residue method is then used to perform the integration over v_z. If the relevant poles of $g(v_z)$ (two in the case of a double resonance, three for the triple resonance) are in the same half of the complex plane, we obtain a zero result which means that the line has the full Doppler width. The condition to have a Doppler-free signal is therefore to have poles in both halves of the complex plane. This condition is directly visualized in the energy-momentum domain diagrams (Fig. 11) ; as a matter of fact, it can be demonstrated

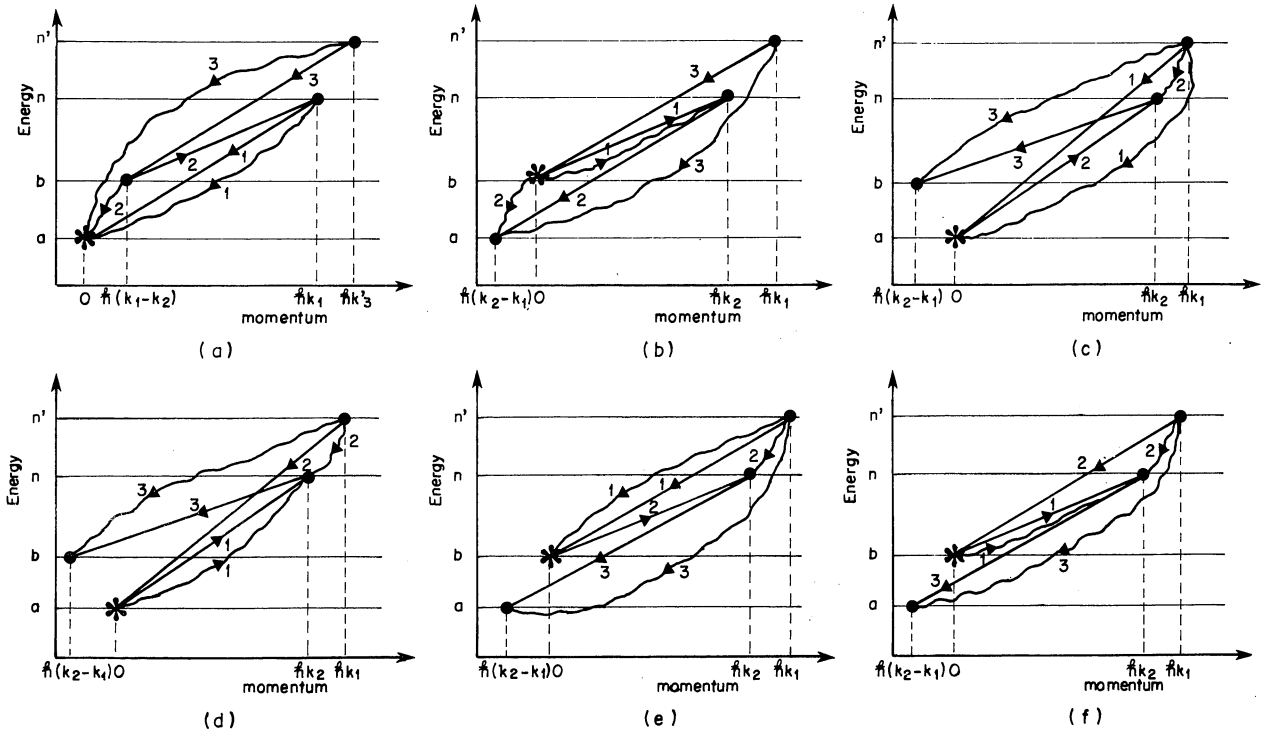

Fig. 11. — Energy-momentum diagrams corresponding to the space-time diagrams of figures 5, 6 ; a, b correspond to figures 5a, 5e and c, d, e, f to figures 6a, 6b, 6c, 6d, respectively.

that the above-mentioned condition is equivalent to having, for the transitions which are near resonance, coherences with wave vectors pointing in opposite directions along the momentum axis [18].

c) *Intensity of Doppler-free lines.* — The two conditions necessary to have Doppler-free lines, *viz.* existence of a selected velocity v_0 *and* coherence requirement (as discussed in 2a, 2b above), do not tell by any means what is the strength of the Doppler-free feature. This strength depends upon the value of v_0 compared to the mean velocity u, through $F(v_0)$ in eq. (26), and is approximately proportional to the Boltzmann factor $e^{-(v_0/u)^2}$. It also depends upon the relative values of the $k_{\alpha\beta}^{(i)}$'s. This aspect will be developed through several examples in the following sections.

3.3.3 *Term depicted in figure* 5e. — The Raman resonant term proportional to $\rho_{bb}^{(0)}$ is depicted by the diagrams of figure 5e and figure 11b. In the same manner as for diagram 5a, the dominant features pertaining to this term are provided by double resonances (a triple resonance is also possible). They will be best interpreted by holding ω_2 near ω_{nb} and tuning ω_1 across $\omega_2 + \omega_{ba}$. When ω_1 is varied, one then observes ω_2-enhanced Raman lines ($\omega_1 - \omega_2 = \omega_{ba}$, $\omega_2 = \omega_{nb}$) and also electronic lines ($\omega_3 = \omega_{n'a}$, $\omega_2 = \omega_{nb}$). There are also anti-Stokes-enhanced Raman lines ($\omega_1 - \omega_2 = \omega_{ba}$, $\omega_{n'a} = \omega_3$) which are

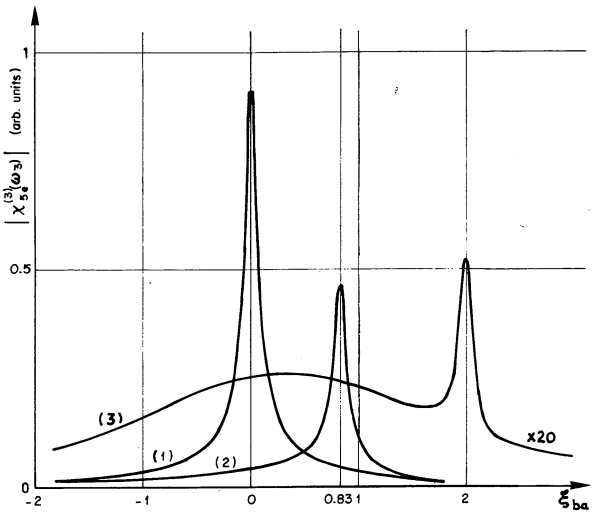

Fig. 12. — ω_2-enhanced Raman line associated with diagram (e) of figure 5.

associated with a set of levels (a, b, n, n') different from that of the other two double resonances. We can tell, just by looking at diagram 11b, that all these lines but the anti-Stokes-enhanced Raman line, are selectively Doppler-free. As an example, we have performed a machine calculation of the profile of the ω_2-enhanced Raman line (Fig. 12). The latter arises from the following term in the susceptibility :

$$\chi_{5e}^{(3)}(\omega_3) = N \frac{\rho_{bb}^{(0)}}{\hbar^3} \times \frac{\mu_{an'}\,\mu_{n'b}\,\mu_{bn}\,\mu_{na}}{\omega_{n'a} - \omega_3 - i\gamma_{n'a}} \times \frac{i\sqrt{\pi}}{(k_1 - k_2)\,k_2\,u^2} \times \frac{w^*(\zeta_{ba}) + w(\zeta_{nb})}{\zeta_{ba}^* - \zeta_{nb}}, \tag{29}$$

with

$$\zeta_{nb} = \frac{\omega_{nb} - \omega_2 + i\gamma_{nb}}{k_2\,u} = \xi_{nb} + i\eta_{nb}\,.$$

The profile of figure 12 has been obtained with parameters $\gamma = \gamma_{na} = \gamma_{nb} = \gamma_{n'a} = \gamma_{ba} = 2\pi\,\Delta\nu_D/40$ and $\xi_{nb} = 0$ (curve 1), $\sqrt{\ln 2}$ (curve 2) and 2 (curve 3). For the three cases, the maximum of the selectively Doppler-free double resonance is at

$$\xi_{ba} = \xi_{nb} = \xi_0 = -\,v_0/u$$

as is expected from eq. (29). We measured the FWHM to be $2\sqrt{3}\,\gamma/2\pi$, which is the expected collisional broadening (i.e. the width of

$$|\,(\omega_{ba} - \omega_1 + \omega_2 - i\gamma_{ba})^{-1}\,|\,;$$

this confirms that the double resonance is Doppler-free. We notice that curve (3) has a second smaller and broader maximum near $\xi_{ba} = 0$; this resonance can also be predicted from the expression for $\chi_{5e}^{(3)}(\omega_3)$ as given in (29). Using

$$\lim w(\zeta)_{|\zeta|\to\infty} = \frac{i\sqrt{\pi}}{\zeta},$$

we obtain from eq. (29) for $\xi_{ba} \simeq 0$, $\xi_{nb} = \xi_0 \gg 0$:

$$\chi_{5e}^{(3)}(\xi_{ba} \simeq 0) = \frac{\rho_{bb}^{(0)}\,\mu_{an'}\,\mu_{n'b}\,\mu_{bn}\,\mu_{na}/\hbar^3}{(\omega_{n'a} - \omega_3 - i\gamma_{n'a})\,(\omega_{nb} - \omega_2 - i\gamma_{nb})} \times \frac{i\sqrt{\pi}}{(k_1 - k_2)\,u}\,w^*(\zeta_{ba})$$

which is exactly the expression for an off-resonance CARS Raman resonance. The resonance at $\xi_{ba} = 0$ is therefore a Doppler-broadened *single* resonance. It is a general feature of third-order nonlinear processes that when $\xi_0 \neq 0$, the line shape arising from a single time-ordered process (i.e. a single diagram) contains two maxima : one selectively Doppler-free double resonance and one Doppler-broadened *single* resonance (this is discussed in the general case in Appendix II). In the case of curves (1) and (2) ξ_0 is either equal to 0 or very close to 0 and the two resonances are mixed.

We can estimate the strength of this type of double resonance in the limit of a very small collisional broadening parameter γ. The maximum CARS line amplitude A_b is obtained from eq. (29) :

$$A_b \propto \frac{N\rho_{bb}^{(0)}}{(k_1 - k_2)\, k_2\, u^2} \times \left| \frac{w^*(\zeta_{ba}) + w(\zeta_{nb})}{\zeta_{ba}^* - \zeta_{nb}} \right|,$$

with

$$\xi_{nb} = \xi_{ba} = -\, v_0/u\,. \tag{30}$$

Adding the condition $\gamma \ll k_{\alpha\beta}^i\, u$ (i.e. $\eta_{nb} \simeq \eta_{ba} \simeq 0$), we have $w(\zeta_{ba}) \simeq w(\zeta_{nb})$ and

$$w(\zeta_{ba}) + w^*(\zeta_{ba}) = 2\ \mathrm{Re}\ w(\zeta_{ba}) \simeq 2\ \mathrm{e}^{-(v_0/u)^2}\,,$$

and thus :

$$A_b \propto N\rho_{bb}^{(0)} \frac{2\ \mathrm{e}^{-(v_0/u)^2}}{\gamma u k_1}\,. \tag{31}$$

For the sake of simplicity, we have assumed equal relaxation rates $\gamma_{na} = \gamma_{ba} = \gamma$, which is certainly not universally valid. Different rates can be easily restored in eq. (31) (see for instance eq. (II.11) of Appendix II).

The line strength is therefore proportional to the Boltzmann factor $\mathrm{e}^{-(v_0/u)^2}$ and inversely proportional to the collisional width γ, and to the Doppler width of the one-photon absorption.

For comparison, we can also calculate the strength of a Doppler-broadened CARS double resonance under the same conditions. We consider, for instance, the double resonance ($\omega_{na} = \omega_1$, $\omega_{ba} = \omega_1 - \omega_2$) associated with figure 5a. We have found in section 1 that the line maximum is at $\xi_{na} = \xi_{ba} = 0$; its amplitude A_a is, using eq. (19) :

$$A_a \propto \frac{N\rho_{aa}^{(0)}}{(k_1 - k_2)\, k_1\, u^2} \left| \frac{w^*(\zeta_{ba}) - w^*(\zeta_{na})}{\zeta_{ba}^* - \zeta_{na}^*} \right|_{\xi_{ba} = \xi_{na} = 0}.$$

Using again the condition $\gamma \ll k_{\alpha\beta}^i\, u$, we have :

$$A_a \propto \frac{N\rho_{aa}^{(0)}}{(k_1 - k_2)\, k_1\, u^2} \mid w'^*(\zeta_{ba}) \mid_{\xi_{ba} = 0, \eta_{ba} \simeq 0} \simeq$$

$$\simeq \frac{N\rho_{aa}^{(0)}}{(k_1 - k_2)\, k_1\, u^2} \times \frac{2}{\sqrt{\pi}}\,. \tag{32}$$

We can now compare the intensities of the Doppler-broadened line and the Doppler-free line using eqs. (31) and (32). Disregarding the magnitudes of the transition moments and of the detuning in the third denominator, we obtain under exact resonance conditions ($\xi_{na} = 0$, $\xi_{nb} = 0$) :

$$\frac{A_b}{A_a} = \frac{\rho_{bb}^{(0)}}{\rho_{aa}^{(0)}} \sqrt{\pi}\, \frac{(k_1 - k_2)\, u}{\gamma}\,,$$

which can be expressed in terms of the approximate widths $2\,\Delta\nu_{\mathrm{D}}$ and $\Delta\nu = \sqrt{3}\,\gamma/\pi$ of the Doppler-broadened and Doppler-free lines, respectively :

$$\frac{A_b}{A_a} \simeq \frac{\rho_{bb}^{(0)}}{\rho_{aa}^{(0)}} \times \frac{\sqrt{\pi}\sqrt{3}}{2\sqrt{\ln 2}} \times \frac{2\,\Delta\nu_{\mathrm{D}}}{\Delta\nu} \simeq 1.8\, \frac{\rho_{bb}^{(0)}}{\rho_{aa}^{(0)}} \times \frac{2\,\Delta\nu_{\mathrm{D}}}{\Delta\nu}\,. \tag{33}$$

Finally, we note that, when performing CARS spectroscopy with ω_1 fixed near ω_{na}, the ($\omega_2 = \omega_{nb}$, $\omega_1 - \omega_2 = \omega_{ba}$) line proportional to $\rho_{bb}^{(0)}$ (Fig. 5e) is located at the same spectral position as the ($\omega_1 = \omega_{na}$, $\omega_1 - \omega_2 = \omega_{ba}$) line proportional to $\rho_{aa}^{(0)}$ (Fig. 5a) ; this is one case where two terms in the susceptibility contribute to the same line in a CARS spectrum. Although $\rho_{bb}^{(0)} < \rho_{aa}^{(0)}$ in most cases, the $\rho_{bb}^{(0)}$ contribution will appear enhanced since it is Doppler-free contrary to that pertaining to $\rho_{aa}^{(0)}$; this will be seen in gases and plasmas at low pressure and high temperature. The triple resonance associated with diagram 5e can also show up in such spectra at the location of the triple resonance associated with diagram 5a (when such a triple resonance occurs).

3.3.4 *Terms depicted in figure* 6. — Looking at the two time-ordered processes giving a contribution proportional to $\rho_{aa}^{(0)}$ (space-time diagrams 6a, 6b and energy-momentum diagrams 11c, 11d) we notice that diagram 11d can give rise to Doppler-free features which are the double resonances ($\omega_{na} = \omega_2$, $\omega_{n'n} = \omega_1 - \omega_2$) and ($\omega_{na} = \omega_2$, $\omega_{n'b} = \omega_3$) ; the last double resonance ($\omega_{n'n} = \omega_1 - \omega_2$, $\omega_{n'b} = \omega_3$) is Doppler-broadened since the wave vectors $k_{n'n}^{(2)}$ and $k_{n'b}^{(3)}$ of the corresponding coherences are pointing in the same direction. Concerning the last two time-ordered processes (space-time diagrams 6c, 6d and energy-momentum diagrams 11e, 11f), only that depicted by figure 11f gives Doppler-free features. These are the ($\omega_2 = \omega_{nb}$, $\omega_3 = \omega_{n'a}$) and ($\omega_2 = \omega_{nb}$, $\omega_1 - \omega_2 = \omega_{n'n}$) double resonances, as well as the triple resonance.

3.3.5 *Strength of a selectively Doppler-free triple resonance.* — Quite generally, we have for the strength of a Doppler-free triple resonance in CARS :

$$|\, \chi^{(3)}(\omega_3)\, | = \frac{N\rho_{\alpha\alpha}^{(0)}}{\hbar^3} \left| \mathscr{M}^{(3)} \int_{-\infty}^{+\infty} \mathrm{d}v_z\, F(v_z)\, \frac{1}{(\Delta\omega_s + k_s v_z + i\gamma_s)\,(\Delta\omega_t + k_t v_z - i\gamma_t)\,(\Delta\omega_r + k_r v_z - i\gamma_r)} \right|, \tag{34}$$

where $\mathscr{M}^{(3)}$ is the product of four transitions moments ; s, t, r indicate the successive coherences established

through the three interactions ; $\Delta\omega$ is the corresponding detuning ; γ and k are the damping factor and wave vector of the coherences, respectively. We can express eq. (34) in terms of the complex error function (eq. (16)) :

$$|\chi^{(3)}(\omega_3)| = \frac{N\rho_{\alpha\alpha}^{(0)}}{\hbar^3}\frac{\sqrt{\pi}}{u^3}\left|\frac{\mathcal{M}^{(3)}}{k_s k_t k_u}\left(\frac{w^*(\zeta_t)}{(\zeta_t^* - \zeta_r^*)(\zeta_t^* - \zeta_s)} + \frac{w^*(\zeta_u)}{(\zeta_r^* - \zeta_t^*)(\zeta_r^* - \zeta_s)} - \frac{w(\zeta_s)}{(\zeta_s - \zeta_t^*)(\zeta_s - \zeta_r^*)}\right)\right|, \quad (35)$$

with

$$\zeta = \xi + i\eta = \frac{\Delta\omega + i\gamma}{ku}.$$

The strength A of the line is given by the value of $|\chi^{(3)}(\omega_3)|$ at the location of the line maximum, which is given by $\xi_s = \xi_t = \xi_r = -v_0/u$ when there exists a velocity v_0 that makes the three denominators in eq. (34) simultaneously minimal. Generalizing the calculation performed in section 3 for the double resonance ($\omega_1 - \omega_2 = \omega_{ba}$, $\omega_{nb} = \omega_2$), we obtain in the limit $\gamma \ll ku$:

$$A = N\frac{\rho_{\alpha\alpha}^{(0)}}{\hbar^3}|\mathcal{M}^{(3)}|\sqrt{\pi}\frac{2\,e^{-(v_0/u)^2}}{u\gamma^2} \times \times \left|\frac{k_s}{(k_s + k_t)(k_s + k_r)}\right|. \quad (36)$$

Here again, one could easily derive a similar formula with different collisional relaxation rates.

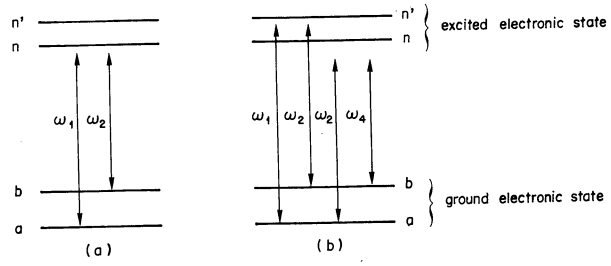

Fig. 13. — Energy level diagrams for SRS and CSRS. ω_1 and ω_2 are the pump frequencies. (a) SRS : one either measures the gain on the signal at ω_2, or the loss at ω_1 ; (b) CSRS : the coherent signal at $\omega_4 = 2\omega_2 - \omega_1$ is monitored.

Using eq. (36), we arrive at the conclusion that the amplitudes of the Doppler-free CARS triple resonances (diagrams, 5e, 6b, 6d) all scale as

$$\frac{e^{-(v_0/u)^2}}{u\gamma^2} \times \frac{k_2}{(k_1)^2}.$$

The expression for the amplitude of any double resonance can also be obtained from eq. (35) using $\lim_{z\to\infty}\frac{w(z)}{z^2} = 0$.

4. **Other third-order nonlinear processes.** — Doppler broadening in three-level systems has been extensively studied by Feld and Javan [24] and Hänsch and Toschek [25]. We here use the diagrammatic representation to analyse the lineshapes in Stimulated Raman Scattering (SRS) and Coherent Stokes Raman Scattering (CSRS) and to identify the terms in the susceptibility which are not subject to Doppler broadening. The resonant transitions involved in these two processes are vizualized in the energy level diagrams of figure 13.

In resonant SRS, ω_1 is tuned near the one-photon absorption frequency ω_{na} and ω_2 is tuned across $\omega_1 - \omega_{ba}$; the Raman gain on the field at ω_2 is monitored and scales as the imaginary part of the Raman susceptibility $\chi^{(3)}(-\omega_2, \omega_2, \omega_1, -\omega_1)$. The space-time diagrams depicting the main contributions to $\chi^{(3)}(\omega_2)$ are shown in figure 14 where the corresponding energy denominators are also indicated. One recognizes the coherent Raman part (diagrams a and d) and the hot luminescence part (diagrams b and c) of the susceptibility [13, 26]. The strongest lines in the

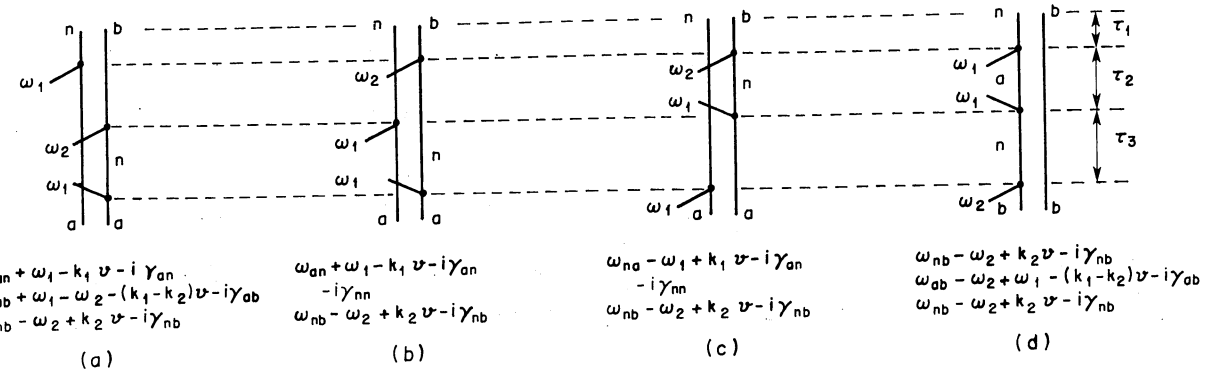

$\omega_{an} + \omega_1 - k_1 v - i\gamma_{an}$
$\omega_{ab} + \omega_1 - \omega_2 - (k_1 - k_2)v - i\gamma_{ab}$
$\omega_{nb} - \omega_2 + k_2 v - i\gamma_{nb}$

$\omega_{an} + \omega_1 - k_1 v - i\gamma_{an}$
$-i\gamma_{nn}$
$\omega_{nb} - \omega_2 + k_2 v - i\gamma_{nb}$

$\omega_{na} - \omega_1 + k_1 v - i\gamma_{an}$
$-i\gamma_{nn}$
$\omega_{nb} - \omega_2 + k_2 v - i\gamma_{nb}$

$\omega_{nb} - \omega_2 + k_2 v - i\gamma_{nb}$
$\omega_{ab} - \omega_2 + \omega_1 - (k_1 - k_2)v - i\gamma_{ab}$
$\omega_{nb} - \omega_2 + k_2 v - i\gamma_{nb}$

Fig. 14. — Diagrammatic representation of the main contributions to $\chi^{(3)}(\omega_2)$; diagram (a) is called *frequency correlation term* in ref. [25], diagrams (b) and (c) correspond to *saturation terms*, and diagram (d) is a dynamic Stark effect. One could also obtain additional contributions by replacing one n by n'.

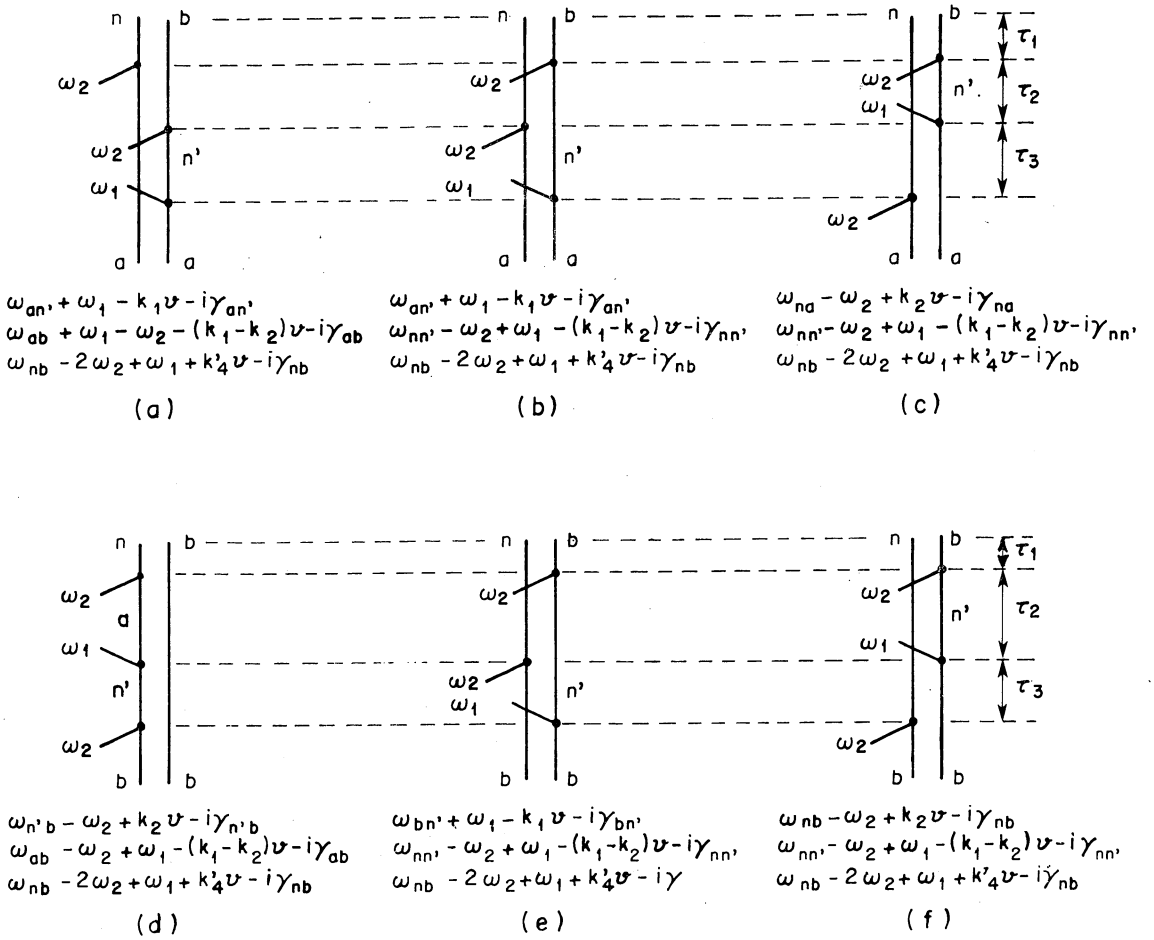

Fig. 15. — Diagrammatic representation of the main contributions to $\chi^{(3)}(\omega_4)$; $k'_4 = 2k_2 - k_1$.

gain spectrum are provided by triple resonances, in contradiction with CARS where triple resonances are only fortuitous.

We have calculated $\varphi(v_z, \tau_1, \tau_2, \tau_3)$ (see eq. (25)) for each of these diagrams :

$$\varphi(v_z, \tau_1, \tau_2, \tau_3) = (-k_1 \tau_3 - (k_1 - k_2)\tau_2 + k_2 \tau_1) v_z , \quad \text{(a)}$$

$$\varphi(v_z, \tau_1, \tau_3) = (-k_1 \tau_3 + k_2 \tau_1) v_z , \quad \text{(b)} \quad (37)$$

$$\varphi(v_z, \tau_1, \tau_3) = (k_1 \tau_3 + k_2 \tau_1) v_z , \quad \text{(c)}$$

$$\varphi(v_z, \tau_1, \tau_2, \tau_3) = (k_2 \tau_3 - (k_1 - k_2)\tau_2 + k_2 \tau_1) v_z , \quad \text{(d)}$$

where a, b, c, d refer respectively to diagrams a, b, c, d. For all the diagrams but c, there exist sets of time intervals (τ_1, τ_2, τ_3) such that $\varphi(v_z, \tau_1, \tau_2, \tau_3) = 0$, and the triple resonances associated with them are therefore Doppler-free.

CSRS is a three-wave mixing process very similar to CARS. The spectrum is representative of the variation of the modulus of the CSRS susceptibility $\chi^{(3)}(-\omega_4, \omega_2, \omega_2, -\omega_1)$ *versus* $(\omega_1 - \omega_2)$ where ω_1 and ω_2 are the pump frequencies $(\omega_2 < \omega_1)$ and $\omega_4 = 2\omega_2 - \omega_1$ is the frequency of the signal. The resonant CSRS spectrum can be obtained with ω_1 set fixed and ω_2 varied or *vice versa*, and the dominant features in the spectrum result from double resonances (or triple resonances when they exist) occurring in some of the terms of the susceptibility $\chi^{(3)}(\omega_4)$. The main ones are shown in figure 15. Diagrams a and d visualize terms possessing the Raman resonant denominator $\omega_{ba} - \omega_1 + \omega_2$; the other four diagrams give terms possessing the two-photon resonance $\omega_{nn'} - \omega_1 + \omega_2$ where $\omega_{nn'}$ is a vibrational frequency in the excited electronic state. The spectral analysis of these resonances is similar to that of CARS and we shall not go into a detailed discussion of them here. Calculating $\varphi(v_z, \tau_1, \tau_2, \tau_3)$ for each diagram of figure 15, we obtain :

$$\varphi(v_z, \tau_1, \tau_2, \tau_3) = (-k_1 \tau_3 - (k_1 - k_2)\tau_2 + k'_4 \tau_1) v_z \quad \text{for diagrams a, b, e ,}$$

$$\varphi(v_z, \tau_1, \tau_2, \tau_3) = (k_2 \tau_3 - (k_1 - k_2)\tau_2 + k'_4 \tau_1) v_z \quad \text{for diagrams c, d, f ,} \quad (38)$$

which shows that all six terms depicted in figure 15 give rise to Doppler-free lines. From the diagrams of figure 15, it is easy to obtain the line shape from the general expression as given in Appendix II (eqs. (II.7) and (II.9)). For each of them, the line shape contains the two resonances (Doppler-free resonance and Doppler-broadened *single* resonance) as discussed in CARS for diagram 5e. We note here that the enhanced Raman line of intensity proportional to the lower vibrational population (diagram 15a) is Doppler-free contrary to the enhanced Raman line obtained in CARS (diagram 5a). The corresponding term in $\chi^{(3)}(\omega_4)$ is :

$$\chi^{(3)}_{15a}(\omega_4) = \rho^{(0)}_{aa} \frac{\mu_{an'}\,\mu_{n'b}\,\mu_{bn}\,\mu_{na}}{\hbar^3} \int_{-\infty}^{+\infty} dv_z\, F(v_z) \frac{1}{\omega_{n'a} - \omega_1 + k_1 v_z + i\gamma_{an'}} \times$$

$$\times \frac{1}{\omega_{ba} - \omega_1 + \omega_2 + (k_1 - k_2) v_z + i\gamma_{ba}} \frac{1}{\omega_{nb} - \omega_4 + k'_4 v_z - i\gamma_{nb}}. \quad (39)$$

The authors of ref. [25] have suggested that the signs of the γ's in this term should all be positive. If such was the case, this enhanced Raman line would be Doppler-broadened ; this is seen readily using the residue theorem as the three poles would lie in the same half of the complex plane. An interesting point is to compare the amplitudes of the above six Doppler-free features in the limit of negligible collisional broadening ($\gamma < ku$). The general formulae given in eqs. (34)-(36) for the maximum amplitude A of a Doppler-free CARS triple resonance can still be used here, because the expressions for $\chi^{(3)}(\omega_3)$ and $\chi^{(3)}(\omega_4)$ are similar (compare for instance eqs. (39) and (34)). The values for k_s, k_t, k_u in eq. (36) can be inferred from eq. (38). In the case of diagrams 15a, b, e, we have $k_s = k'_4 = 2k_2 - k_1$, $k_t = k_1$, $k_u = k_1 - k_2$, so that the strengths of the features associated with them scale as :

$$A_{a,b,e} \sim \frac{2 \exp - (v_0/u)^2}{u\gamma^2} \frac{2k_2 - k_1}{2k_2^2}.$$

For diagrams 15c, d, f, we have $k_s = k_1 - k_2$, $k_t = k_2$, $k_u = k'_4$ and the strengths of the corresponding features scale as :

$$A_{c,d,f} \sim \frac{2 \exp - (v_0/u)^2}{u\gamma^2} \frac{k_1 - k_2}{k_1 k_2},$$

which is about $(\omega_{na}/\omega_{ba})$ times smaller than that of the former features. Here again, the strengths $A_{a,b,e}$, and $A_{c,d,f}$ could be calculated in the general case of distinct collisional parameters γ_{na}, γ_{nb}, γ_{ba}... as is done in Appendix II.

5. **Conclusion.** — We have analysed the theory of CARS at electronic resonance in gases under conditions of mixed line broadening. We used two time-ordered diagrammatic representations of the non-linear susceptibility terms. A representation in the space-time domain, associated with a proper set of diagrammatic rules, has enabled us to perform a direct calculation of the most important terms, from which the line shapes could be calculated. A representation in the energy-momentum domain was also used for a rapid identification of those terms which are associated with Doppler-free time-ordered processes.

This analysis has led us to several important findings :

(i) The CARS susceptibility term which dominates in the collision regime is not Doppler-free under double resonance condition and even under triple resonance condition.

(ii) The terms which are Doppler-free usually give smaller contributions in the collision regime, either because their population factor is small ($\rho^{(0)}_{bb}$ terms) or because their individual contributions cancel (terms containing excited electronic states vibrational resonances). In the Doppler regime, all these terms are responsible for spectral resonances whose widths are of the order of the collisional linewidth and whose amplitudes become comparable to those of the Doppler-broadened resonances (i).

(iii) The Doppler-free character of a susceptibility term is given by the existence of a particular velocity group which simultaneously minimizes two or three of the resonance denominators *and* by the in-phase, cooperative nature of the contributions to the associated time-ordered process from nearby velocity groups. We have called these Doppler-free processes *selectively Doppler-free* in contrast with processes such as two-photon absorption which can be truly Doppler-free and involve the participation of all velocity groups.

This analysis has also been extended to other non-linear processes such as CSRS and stimulated Raman scattering ; most of the terms which dominate in the collision regime are also selectively Doppler-free. These two techniques are therefore better suited than CARS for the high-resolution Raman spectroscopy of gases.

Weak elastic collisions could also be included in this diagrammatic approach of CARS line shapes, by taking the Fourier transform of the density operator evolution equation with respect to axial velocity, as was done for saturated absorption spectro-

scopy [28]. Finally, other nonlinear spectroscopic techniques such as RIKES [29], which involve distinct polarization vectors for the applied electric fields can be readily handled by the formalism of Appendix II and reference [20].

Acknowledgments. — The authors wish to thank Ms. B. Attal for very helpful discussions concerning the identification of the time-ordered processes of interest in resonant CARS, as well as Dr. M. M. Roberge and Prof. T. K. Gustafson.

Appendix I. — The density operator $\rho'(z', t', v_z)$ for the class of molecules having velocity v_z along the z axis, written in the molecular frame of reference, is a solution of the evolution equation :

$$\frac{\partial \rho'(z', t', v_z)}{\partial t'} + R(\rho'(z', t', v_z) - \rho^{(0)}) = \frac{-i}{\hbar}[H_0 + V'(z', t'), \rho'(z', t', v_z)] \tag{I.1}$$

where $R\rho'$ represents the relaxation processes towards the equilibrium density operator $\rho^{(0)}$ and where $V'(z', t')$ is the interaction Hamiltonian :

$$V'(z', t') = -\boldsymbol{\mu} . \boldsymbol{\mathcal{E}}'(z', t') ;$$

$\boldsymbol{\mathcal{E}}'(z', t')$ is the electric field expressed in the molecular frame. We can obtain $\boldsymbol{\mathcal{E}}'(z', t')$ from $\boldsymbol{\mathcal{E}}(z, t)$ as given in eq. (1) using the Galilean transformation from the molecular to the laboratory frame :

$$\left.\begin{aligned} t &= t' \\ z &= z' + v_z t' \end{aligned}\right\} . \tag{I.2}$$

We have thus :

$$\boldsymbol{\mathcal{E}}'(z', t') = \boldsymbol{\mathcal{E}}(z = z' + v_z t', t = t') .$$

For the field interaction represented by the one-vertex diagram of figure 2a, the integration of eq. (I.1) leads to :

$$\rho'^{(n+1)}_{\alpha\beta}(z', t', v_z) = \frac{i\mu_{\alpha\alpha'} E_j}{2\hbar} e^{-i\omega_j t'} e^{ik_j(z' + v_z t')} e^{i\varphi_j} \times \int_0^\infty d\tau\, e^{-i(\omega_{\alpha\beta} - i\gamma_{\alpha\beta})\tau} e^{i(\omega_j - k_j v_z)\tau} \rho'^{(n)}_{\alpha'\beta}(z', t' - \tau, v_z) . \tag{I.3}$$

The expression $\rho^{(n+1)}_{\alpha\beta}(z, t, v_z)$ for the density matrix element in the laboratory frame is then obtained from eq. (I.3) using the Galilean transformation (I.2) :

$$\rho^{(n+1)}_{\alpha\beta}(z, t, v_z) = \rho'^{(n+1)}_{\alpha\beta}(z' = z - v_z t, t' = t, v_z) = \frac{i\mu_{\alpha\alpha'} E_j}{2\hbar} e^{-i\omega_j t} \times$$

$$\times e^{ik_j z} e^{i\varphi_j} \int_0^\infty d\tau\, e^{-i(\omega_{\alpha\beta} - i\gamma_{\alpha\beta})\tau} e^{i(\omega_j - k_j v_z)\tau} \rho'^{(n)}_{\alpha'\beta}(z - v_z t, t - \tau, v_z) . \tag{I.4}$$

Using again $\rho'^{(n)}_{\alpha'\beta}(z - v_z t, t - \tau, v_z) = \rho^{(n)}_{\alpha'\beta}(z - v_z \tau, t - \tau, v_z)$, we get eq. (10) in the text.

A more general derivation using a Lorentz transformation between frames, and using density matrix elements between energy-momentum states will be found in ref. [18].

Appendix II. — GENERAL EXPRESSION FOR A THIRD-ORDER NONLINEAR POLARIZATION. — The results of the present paper can be extended to all nonlinear processes. We give here a brief account of this generalization which will be presented in more detail in [18].

We shall derive the general expression for the polarization corresponding to the nonlinear process represented by the diagram of figure II.1 which includes all possibilities of interactions with three different waves coming from both directions along the same z axis. To gather all possibilities of choices between vertices on the first or on the second column we write the transition moments with Liouville space notation :

$$\mu_{\alpha_s\beta_s,\alpha_r\beta_r} = \mu_{\alpha_s\alpha_r} \delta_{\beta_r\beta_s} - \mu_{\beta_r\beta_s} \delta_{\alpha_r\alpha_s} . \tag{II.1}$$

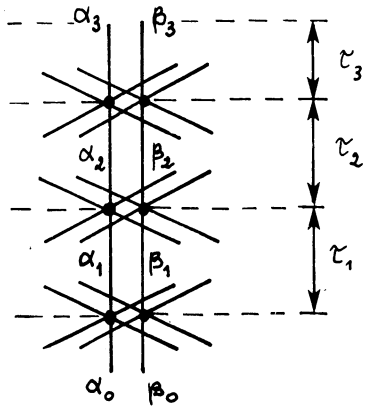

Fig. II.1. — General diagram for a third-order process with three different waves coming from both directions.

At each perturbation order r, the interacting field component is written :

$$\tfrac{1}{2}\,\hat{e}_r(\varepsilon'_r)\,E_r \exp[\varepsilon'_r\, i(\omega_r\, t - \varepsilon''_r\, k_r\, z - \varphi_r)]$$

with :

$$\varepsilon'_r = \pm 1\,, \qquad \varepsilon''_r = \pm 1\,, \qquad \hat{e}_r(+1) = \hat{e}_r\,, \qquad \hat{e}_r(-1) = \hat{e}^*_r\,.$$

The complex nonlinear electric polarization corresponding to this very general diagram is given by :

$$\mathbf{P}^{(3)} = 2\,N\boldsymbol{\mu}_{\beta_3\alpha_3}\,\rho^{(3)}_{\alpha_3\beta_3} \tag{II.2}$$

where $\rho^{(3)}_{\alpha_3\beta_3}$ is obtained by simple application of the diagrammatic rules :

$$\begin{aligned}\rho^{(3)}_{\alpha_3\beta_3} = \int_{-\infty}^{+\infty} \mathrm{d}v_z\, F(v_z) \int_0^{\infty} \mathrm{d}\tau_1 \int_0^{\infty} \mathrm{d}\tau_2 \int_0^{\infty} \mathrm{d}\tau_3 \times \\ \times\, i[\boldsymbol{\mu}.\hat{e}_3(\varepsilon'_3)]_{\alpha_3\beta_3,\alpha_2\beta_2}(E_3/2\,\hbar) \exp[-(i\omega_{\alpha_3\beta_3} + \gamma_{\alpha_3\beta_3})\,\tau_3] \\ \times \exp\{\varepsilon'_3\, i[\omega_3(t-\tau_3) - \varepsilon''_3\, k_3(z - v_z\,\tau_3) - \varphi_3]\} \\ \times\, i[\boldsymbol{\mu}.\hat{e}_2(\varepsilon'_2)]_{\alpha_2\beta_2,\alpha_1\beta_1}(E_2/2\,\hbar) \exp[-(i\omega_{\alpha_2\beta_2} + \gamma_{\alpha_2\beta_2})\,\tau_2] \\ \times \exp\{\varepsilon'_2\, i[\omega_2(t-\tau_3-\tau_2) - \varepsilon''_2\, k_2(z - v_z(\tau_3+\tau_2)) - \varphi_2]\} \\ \times\, i[\boldsymbol{\mu}.\hat{e}_1(\varepsilon'_1)]_{\alpha_1\beta_1,\alpha_0\beta_0}(E_1/2\,\hbar) \exp[-(i\omega_{\alpha_1\beta_1} + \gamma_{\alpha_1\beta_1})\,\tau_1] \\ \times \exp\{\varepsilon'_1\, i[\omega_1(t-\tau_3-\tau_2-\tau_1) - \varepsilon''_1\, k_1(z - v_z(\tau_3+\tau_2+\tau_1)) - \varphi_1]\}\,\rho^{(0)}_{\alpha_0\beta_0}\,,\end{aligned} \tag{II.3}$$

where $\rho^{(0)}_{\alpha_0\beta_0}$ contains an implicit $\delta_{\alpha_0\beta_0}$ to represent an equilibrium population.

Quite generally the $\mathbf{P}^{(3)}.\hat{e}_4$ component of the nonlinear complex polarization is proportional to the quantity :

$$[\boldsymbol{\mu}.\hat{e}_4]_{\beta_3\alpha_3}[\boldsymbol{\mu}.\hat{e}_3(\varepsilon'_3)]_{\alpha_3\beta_3,\alpha_2\beta_2}[\boldsymbol{\mu}.\hat{e}_2(\varepsilon'_2)]_{\alpha_2\beta_2,\alpha_1\beta_1}[\boldsymbol{\mu}.\hat{e}_1(\varepsilon'_1)]_{\alpha_1\beta_1,\alpha_0\beta_0}$$

which can be easily calculated in the general case of arbitrary polarization vectors $\hat{e}_r$ and degenerate levels following the method of reference [20]. In the present paper we have assumed the fields to have a common linear polarization $\hat{e}$ and non-degenerate levels for simplicity so that the previous quantity will be written :

$$\mathcal{M}^{(3)} = \mu_{\beta_3\alpha_3}\,\mu_{\alpha_3\beta_3,\alpha_2\beta_2}\,\mu_{\alpha_2\beta_2,\alpha_1\beta_1}\,\mu_{\alpha_1\beta_1,\alpha_0\beta_0}\,. \tag{II.4}$$

We get therefore the following third-order polarization :

$$\begin{aligned}P^{(3)} = \mathbf{P}^{(3)}.\hat{e} = -\,iN\rho^{(0)}_{\alpha_0\beta_0}(\mathcal{M}^{(3)}/4\,\hbar^3)\,E_1\,E_2\,E_3 \exp[-i(\omega^{(3)}\,t - k^{(3)}\,z - \varphi^{(3)})] \times \\ \times \int_{-\infty}^{+\infty} \mathrm{d}v_z\, F(v_z)\,[-i(\omega^{(1)} - \omega_{\alpha_1\beta_1} + i\gamma_{\alpha_1\beta_1} - k^{(1)}\,v_z)]^{-1} \\ \times\,[-i(\omega^{(2)} - \omega_{\alpha_2\beta_2} + i\gamma_{\alpha_2\beta_2} - k^{(2)}\,v_z)]^{-1}\,[-i(\omega^{(3)} - \omega_{\alpha_3\beta_3} + i\gamma_{\alpha_3\beta_3} - k^{(3)}\,v_z)]^{-1}\,,\end{aligned} \tag{II.5}$$

with

$$\omega^{(r)} = -\sum_{j=1}^{r} \varepsilon'_j\,\omega_j\,, \qquad k^{(r)} = -\sum_{j=1}^{r} \varepsilon'_j\,\varepsilon''_j\,k_j\,, \qquad \varphi^{(r)} = -\sum_{j=1}^{r} \varepsilon'_j\,\varphi_j\,.$$

If we introduce the notations :

$$\zeta_{\alpha_r\beta_r} = \xi_{\alpha_r\beta_r} + i\eta_{\alpha_r\beta_r} = (\omega^{(r)} - \omega_{\alpha_r\beta_r} + i\gamma_{\alpha_r\beta_r})/k^{(r)}\,u\,,$$

$$\theta = v_z/u\,,$$

the susceptibility contribution can be written :

$$\chi^{(3)} = -\,iN\rho^{(0)}_{\alpha_0\alpha_0}(\mathcal{M}^{(3)}/\hbar^3\sqrt{\pi}\,k^{(1)}\,k^{(2)}\,k^{(3)}\,u^3) \times$$

$$\times \int_{-\infty}^{+\infty} d\theta[(-\,i\zeta_{\alpha_1\beta_1} + i\theta)\,(-\,i\zeta_{\alpha_2\beta_2} + i\theta)\,(-\,i\zeta_{\alpha_3\beta_3} + i\theta)]^{-1}\exp(-\,\theta^2)\,. \qquad \text{(II.6)}$$

The θ integral is calculated as usual :

$$\int_{-\infty}^{+\infty} d\theta(-\,i\zeta_{\alpha\beta} + i\theta)^{-1}\exp(-\,\theta^2) = \pi w(\zeta_{\alpha\beta}) \qquad \text{if} \quad k^{(r)} > 0\,,$$

$$\int_{-\infty}^{+\infty} d\theta(-\,i\zeta_{\alpha\beta} + i\theta)^{-1}\exp(-\,\theta^2) = -\,\pi w(-\,\zeta_{\alpha\beta}) \quad \text{if} \quad k^{(r)} < 0\,.$$

If we define $\varepsilon_r = k^{(r)}/|\,k^{(r)}\,|$ we get :

$$\chi^{(3)} = (i\sqrt{\pi}\,N\rho^{(0)}_{\alpha_0\alpha_0}\,\mathcal{M}^{(3)}/\hbar^3\,k^{(1)}\,k^{(2)}\,k^{(3)}\,u^3) \times$$

$$\times\left[\frac{\varepsilon_1\,w(\varepsilon_1\,\zeta_{\alpha_1\beta_1})}{(\zeta_{\alpha_2\beta_2} - \zeta_{\alpha_1\beta_1})\,(\zeta_{\alpha_3\beta_3} - \zeta_{\alpha_1\beta_1})} + \frac{\varepsilon_2\,w(\varepsilon_2\,\zeta_{\alpha_2\beta_2})}{(\zeta_{\alpha_1\beta_1} - \zeta_{\alpha_2\beta_2})\,(\zeta_{\alpha_3\beta_3} - \zeta_{\alpha_2\beta_2})} + \frac{\varepsilon_3\,w(\varepsilon_3\,\zeta_{\alpha_3\beta_3})}{(\zeta_{\alpha_1\beta_1} - \zeta_{\alpha_3\beta_3})\,(\zeta_{\alpha_2\beta_2} - \zeta_{\alpha_3\beta_3})}\right], \qquad \text{(II.7)}$$

or in a form which can be generalized to higher perturbation order :

$$\chi^{(3)} = (-\,i(-\,1)^3\sqrt{\pi}\,N\rho^{(0)}_{\alpha_0\alpha_0}\,\mathcal{M}^{(3)}/\hbar^3\,u^3)\sum_{r=1}^{3} w(\varepsilon_r\,\zeta_{\alpha_r\beta_r})/|\,k^{(r)}\,|\prod_{s=1,s\neq r}^{3} k^{(s)}(\zeta_{\alpha_s\beta_s} - \zeta_{\alpha_r\beta_r})\,. \qquad \text{(II.8)}$$

The total polarization of the medium is finally obtained by summing over all possibilities to choose the successive α_r, β_r and the three fields.

We now show that Doppler-free processes require either one $k^{(r)} \equiv 0$ or two opposite ε_r.

If one of the $k^{(r)} \to 0$ the corresponding term in the previous sum disappears and we are left with :

$$\chi^{(3)} = \frac{i\sqrt{\pi}\,N\rho^{(0)}_{\alpha_0\alpha_0}\,\mathcal{M}^{(3)}/\hbar^3}{\omega^{(r)} - \omega_{\alpha_r\beta_r} + i\gamma_{\alpha_r\beta_r}}\left[\frac{\varepsilon_s\,w(\varepsilon_s\,\zeta_{\alpha_s\beta_s}) - \varepsilon_t\,w(\varepsilon_t\,\zeta_{\alpha_t\beta_t})}{k^{(s)}\,k^{(t)}\,u^2(\zeta_{\alpha_t\beta_t} - \zeta_{\alpha_s\beta_s})}\right], \qquad \text{(II.9)}$$

where the first denominator gives a true Doppler-free resonance when $\omega^{(r)}$ can be tuned through $\omega_{\alpha_r\beta_r}$. This is the case of Doppler-free two-photon spectroscopy for example. If $\xi_{\alpha_s\beta_s}$ and $\xi_{\alpha_t\beta_t}$ are simultaneously very large but different from each other, when $\omega^{(r)} \simeq \omega_{\alpha_r\beta_r}$ the asymptotic approximation $w(\zeta) = i/\sqrt{\pi}\,\zeta$ gives the usual expression :

$$\chi^{(3)} \sim -\,\frac{N\rho^{(0)}_{\alpha_0\alpha_0}\,\mathcal{M}^{(3)}/\hbar^3}{\omega^{(r)} - \omega_{\alpha_r\beta_r} + i\gamma_{\alpha_r\beta_r}}\left[\frac{1}{(\omega^{(t)} - \omega_{\alpha_t\beta_t})\,(\omega^{(s)} - \omega_{\alpha_s\beta_s})}\right]. \qquad \text{(II.10)}$$

A double resonance is obtained for $\xi_{\alpha_t\beta_t} = \xi_{\alpha_s\beta_s} = \xi_0$ as can be seen on the second denominator of eq. (II.9) ; this implies that a given velocity group v_0, such that $\theta_0 = \xi_0$, cancels the real part of two denominators in eq. (II.6). This double resonance is also obtained when $k^{(r)} \neq 0$ if $|\,\xi_{\alpha_r\beta_r}\,| \gg |\,\xi_0\,|$ as eq. (II.9) is still valid under those conditions. This double resonance may be selectively Doppler-free or Doppler broadened as we shall now see. In the Doppler limit ($\eta \to 0$) we may use :

$$w(\xi + i\eta) \sim w(\xi) = e^{-\xi^2}\left(1 + \frac{2\,i}{\sqrt{\pi}}\int_0^{\xi} e^{-t^2}\,dt\right)$$

and expression (II.9) gives at location $\xi_{\alpha_s\beta_s} = \xi_{\alpha_t\beta_t} = \xi_0$:

$$\chi^{(3)}(\xi_0) = \frac{\sqrt{\pi}\,N\rho^{(0)}_{\alpha_0\alpha_0}\,\mathcal{M}^{(3)}/\hbar^3}{\omega^{(r)} - \omega_{\alpha_r\beta_r} + i\gamma_{\alpha_r\beta_r}}\,\frac{(\varepsilon_s - \varepsilon_t)\exp(-\,\xi_0^2)}{k^{(s)}\,u\gamma_{\alpha_t\beta_t} - k^{(t)}\,u\gamma_{\alpha_s\beta_s}}, \qquad \text{(II.11)}$$

which differs from zero only if $\varepsilon_s = -\varepsilon_t$ and has a non-negligible amplitude only if ξ_0 is not too large because of the factor $\exp(-\xi_0^2)$. If $\xi_0 \gg 0$, one obtains in addition to the selectively Doppler-free double resonance two Doppler-broadened resonances located at $\xi_{\alpha_s\beta_s} \simeq 0$ and $\xi_{\alpha_t\beta_t} \simeq 0$ owing to the factors w at the numerator of eq. (II.9). For example, in the vicinity of $\xi_{\alpha_s\beta_s} = 0$ we may write :

$$\chi^{(3)} \sim \frac{i\sqrt{\pi}\, N\rho^{(0)}_{\alpha_0\alpha_0}\, \mathcal{M}^{(3)}/\hbar^3}{(\omega^{(r)} - \omega_{\alpha_r\beta_r})\,(\omega^{(t)} - \omega_{\alpha_t\beta_t})\,|k^{(s)}|\,u}\, w(\varepsilon_s\, \zeta_{\alpha_s\beta_s})\,, \tag{II.12}$$

which is the usual expression for off-resonance CARS or Doppler-free two-photon spectroscopy with unequal frequencies ; this is the reason why we label the corresponding Doppler-broadened resonance, *single* resonance. As ξ_0 increases, the selectively Doppler-free double resonance is more and more shifted from positions $\xi_{\alpha_s\beta_s} \simeq 0$, $\xi_{\alpha_t\beta_t} \simeq 0$ and reduced, and the Doppler-broadened *single* resonances acquire an increasing contrast. This situation is illustrated in the main text by the double-resonance and *single* resonance associated with diagram 5e.

If $\varepsilon_s = \varepsilon_t = \varepsilon$ the amplitude of $\chi^{(3)}$ for a double-resonance can still be obtained by expanding the error function to first order in η :

$$w(\xi + i\eta) \sim w(\xi) + i\eta w'(\xi)$$

with [23]

$$w'(\zeta) = -2\,\zeta w(\zeta) + \frac{2\,i}{\sqrt{\pi}}\,.$$

We get at position $\xi_{\alpha_s\beta_s} = \xi_{\alpha_t\beta_t} = \xi_0$:

$$\chi^{(3)}(\xi_0) = -\frac{i\sqrt{\pi}\, N\rho^{(0)}_{\alpha_0\alpha_0}\, \mathcal{M}^{(3)}/\hbar^3}{(\omega^{(r)} - \omega_{\alpha_r\beta_r} + i\gamma_{\alpha_r\beta_r})\, k^{(s)}\, u\, k^{(t)}\, u}\, \varepsilon w'(\varepsilon\xi_0)\,, \tag{II.13}$$

which is smaller than the amplitude of the selectively Doppler-free double-resonance by a factor of the order of γ/ku, and has therefore the same order of magnitude as the signal away from the double-resonance position. No strong resonance will thus emerge at ξ_0. This situation is illustrated in the main text by the double resonance associated with diagram 5a.

When the three detunings $\xi_{\alpha_r\beta_r}$, $\xi_{\alpha_s\beta_s}$, $\xi_{\alpha_t\beta_t}$ have the same order of magnitude and when all $k^{(r)}$'s are different from zero, the general formula (II.7) should be used. A triple resonance is obtained whenever the double condition $\xi_{\alpha_r\beta_r} = \xi_{\alpha_s\beta_s} = \xi_{\alpha_t\beta_t} = \xi_0$ can be satisfied. Two of the ε_r have the same value, for example, $\varepsilon_r = \varepsilon_s = \varepsilon$; in the Doppler limit we get :

$$\chi^{(3)}(\xi_0) = -\frac{i\sqrt{\pi}\, N\rho^{(0)}_{\alpha_0\alpha_0}\, \mathcal{M}^{(3)}/\hbar^3}{k^{(r)}\, k^{(s)}\, k^{(t)}\, u^3}\, \frac{(\varepsilon_t - \varepsilon)\exp(-\xi_0^2)}{(\eta_t - \eta_r)\,(\eta_t - \eta_s)}\,, \tag{II.14}$$

which differs from zero only if $\varepsilon_t = -\varepsilon$.

If $\varepsilon_t = \varepsilon$ we can use the expansion of $w(\zeta)$ to second order in η :

$$w(\xi + i\eta) \sim w(\xi) + i\eta w'(\xi) - \frac{\eta^2}{2}\, w''(\xi)$$

with [23]

$$w''(\zeta) = -2\,\zeta w'(\zeta) - 2\,w(\zeta)$$

and we get for ξ_0 :

$$\chi^{(3)}(\xi_0) = \frac{i\sqrt{\pi}\, N\rho^{(0)}_{\alpha_0\alpha_0}\, \mathcal{M}^{(3)}/\hbar^3}{2\, k^{(r)}\, k^{(s)}\, k^{(t)}\, u^3}\, \varepsilon w''(\varepsilon\xi_0)\,, \tag{II.15}$$

which is smaller than the selectively Doppler-free triple resonance by a factor of the order of $\gamma^2/(ku)^2$, and thus cannot emerge from the background.

These expressions and considerations are applicable to all nonlinear processes : saturation spectroscopy, two-photon spectroscopy, CARS, CSRS and SRS, etc...

References

[1] NIBLER, J. W. and KNIGHTEN, G. V., Coherent anti-Stokes Raman Spectroscopy, in *Topics in Current Physics*, Ed. by A. Weber (Springer Verlag, New York) 1977.

[2] DRUET, S. and TARAN, J.-P., Coherent anti-Stokes Raman Spectroscopy, in *Chemical and Biochemical Applications of Lasers*, Vol. **4**, ed. by C. B. Moore (Academic Press, New York) 1979.

[3] HENESSIAN, M. A., KULEVSKII, L. and BYER, R. L., *J. Chem. Phys.* **65** (1976) 5530.

[4] HENESSIAN, M. A., KULEVSKII, L., BYER, R. L. and HERBST, R. L., *Opt. Commun.* **18** (1976) 225.

[5] HIRTH, A. and VOLRATH, K., *Opt. Commun.* **18** (1976) 213.

[6] BOQUILLON, J.-P., MORET-BAILLY, J. and CHAUX, R., *C.R. Hebd. Séan. Acad. Sci.* Paris **B 284** (1977) 205.

[7] FABELINSKY, V. I., KRYNETSKY, B. B., KULEVSKY, L. A., MISHIN, V. A., PROKHOROV, A. M., SAVEL'EV, A. D. and SMIRNOV, V. V., *Opt. Commun.* **20** (1977) 398.

[8] BERGER, H., *Opt. Commun.* **25** (1978) 179.

[9] HENESSIAN, M. A. and BYER, R. L., *J. Opt. Soc. Am.* **68** (1978) 648.

[10] ROH, W. B., WEBER, R. F. and SCHREIBER, P. W., *Opt. Commun.* **27** (1978) 142.

[11] ATTAL, B., SCHNEPP, O. O. and TARAN, J.-P. E., *Opt. Commun.* **24** (1978) 77.

[12] DRUET, S. A. J., ATTAL, B., GUSTAFSON, T. K. and TARAN, J.-P. E., *Phys. Rev.* **A 18** (1978) 1529.

[13] YEE, S. Y., GUSTAFSON, T. K., DRUET, S. A. J., and TARAN, J.-P. E., *Opt. Commun.* **23** (1977) 1.

[14] BORDÉ, C. J., HALL, J. L., KUNASZ, C. V. and HUMMER, D. G., *Phys. Rev.* **A 14** (1976) 236.

[15] BORDÉ, C. J., *C.R. Hebd. Séan. Acad. Sci.* Paris **282B** (1976) 341.

[16] BORDÉ, C. J., in *Laser Spectroscopy III, Proceedings of the Third International Conference*, Jackson Lake Lodge, USA, July 4-8, 1978, ed. by J. L. Hall and J. L. Carlsten (Springer-Verlag, Berlin, New York) 1977, p. 121.

[17] BORDÉ, C. J., CAMY, G. and DECOMPS, B., *Phys. Rev.* (1979), in press.

[18] BORDÉ, C. J., *Density matrix equations and diagrams for high resolution laser spectroscopy*, to be published.

[19] BLOEMBERGEN, N., LOTEM, H. and LYNCH, Jr., R. T., *Indian J. Pure Appl. Phys.* **16** (1978) 151.

[20] BORDÉ, J. and BORDÉ, C. J., *J. Mol. Spectrosc.* (1979), in press.

[21] CAGNAC, B., GRYNBERG, G. and BIRABEN, F., *J. Physique* **34** (1973) 56.

[22] GRYNBERG, G., BIRABEN, F., BASSINI, M. and GAGNAC, B., *Phys. Rev. Lett.* **37** (1976) 283.

[23] ABRAMOWITZ, M. and STEGUN, I. A., *Handbook of mathematical functions* (Dover, New York) 1965.

[24] FELD, M. S. and JAVAN, A., *Phys. Rev.* **177** (1969) 540.

[25] HÄNSCH, Th. and TOSCHEK, P., *Z. Phys.* **236** (1970) 213.

[26] SHEN, Y. R., *Phys. Rev.* **139** (1974) 622.

[27] CARREIRA, L. A., GOSS, L. P. and MALLOY, Jr., T. B., *J. Chem. Phys.* **69** (1978) 855.

[28] BORDÉ, C. J., AVRILLIER, S. and GORLICKI, M., *J. Physique Lett.* **38** (1977) L-249.

[29] HEIMAN, D., HELLWARTH, R. W., LEVENSON, M. D. and MARTIN, G., *Phys. Rev. Lett.* **36** (1976) 189.